JMEPEG (2023) 32:8517–8540
https://doi.org/10.1007/s11665-023-08233-5

1059-9495/$19.00

REVIEW

A Review of High-Strength Aluminum-Copper Alloys Fabricated by Wire Arc Additive Manufacturing: Microstructure, Properties, Defects, and Post-processing

Siyue Fan, Xuming Guo, Zhenhua Li, Jing Ma, Fei Li, and Qingwei Jiang

Submitted: 28 February 2023 / Revised: 27 March 2023 / Accepted: 1 April 2023 / Published online: 10 May 2023

Wire arc additive manufacturing (WAAM) techniques have been gaining increasing attention in the contemporary manufacturing sector due to their advantages in economically producing large-sized metallic components with relatively high deposition rates. High-strength Al-Cu alloys are widely used in aerospace, military, and automotive industries applications due to their high specific strength and excellent processability. WAAM offers an efficient way to produce large-sized high-strength Al-Cu alloy components, and the related field is rapidly evolving. This article reviews the current research for WAAM high-strength Al-Cu alloys on the manufacturing process, solidification microstructure, common defects, mechanical properties, and post-processing processes. Research findings have been positive regarding the microstructure and mechanical properties of WAAM high-strength Al-Cu alloys. Finally, this article outlines the development prospects of WAAM high-strength Al-Cu alloys based on the previous research.

Keywords defects, Al-Cu alloy, microstructure, quality improvement, wire arc additive manufacturing

1. Introduction

Metal material manufacturing field is a crucial component of modern industrial society and a reflection of national creativity, competitiveness, and comprehensive national power (Ref 1, 2). Recently, additive manufacturing (AM) provides new pathways and opportunities for the metal material manufacturing field (Ref 3-5). In the AM process, parts are constructed layer-by-layer using a 3D digital model based on the principle of discrete stacking (Ref 6). Among the various AM technologies, wire arc additive manufacturing (WAAM) stands out due to its advantages of low materials cost and high deposition efficiency (Ref 7-9). Today, WAAM is being used as a promising fabrication process for large-sized and low-complexity metallic components, and a range of engineering materials such as titanium, aluminum, copper, and steel have been utilized (Ref 10-13).

The 2xxx-series high-strength Al-Cu alloys (hereafter referred to as Al-Cu alloy) are the key lightweight structural materials in the aerospace, military, and automotive industries due to their high specific strength, excellent processability, and age-hardening ability (Ref 14-16). Using WAAM to produce Al-Cu alloys has obvious advantages: (1) Multiple manufacturing processes are simplified into one, enabling integral forming of materials, and thus reducing production costs and cycle and (2) multiple parts can be designed as one, giving more space for innovation and thereby improving design flexibility. According to reports, the WAAM system resulted in a massive 64% reduction in the cycle time, compared with traditional subtractive manufacturing processes (Ref 17). Therefore, the application of WAAM process to manufacture high-strength Al-Cu alloys has become a popular research topic.

Over the past decade, lots of studies have been developed focusing on Al-Cu alloy fabricated by WAAM, and these research enthusiasms continue to rise. Al-Cu alloys have been considered by researchers as one of the most suitable materials for the application of WAAM. Significant research has been carried out to (1) optimize the WAAM processes to improve efficiency and quality, (2) develop new wires to improve microstructure, and (3) design post-processing processes to enhance mechanical properties and minimize defects. Although there have been numerous studies that demonstrated the potential of Al-Cu alloy fabricated by WAAM, only a small number of papers summarized the development in WAAM for aluminum alloys and there is not enough for the summary of the current development in WAAM for Al-Cu alloys, which was the main motivation for writing this paper. This is very necessary because it can provide new ideas for the subsequent development.

This paper reviews the current development of Al-Cu alloy fabricated by WAAM, including the manufacturing processes, solidification microstructure, common defects, mechanical properties, and post-processing processes. Additionally, the effective methods for quality improvement and defects minimization are also discussed. Finally, the future research prospects for Al-Cu alloy fabricated by WAAM are outlined.

Siyue Fan, School of Materials Science and Engineering, Kunming University of Science and Technology, Kunming 650000, China; and Yunnan Innovation Institute of Beihang University, Kunming 650000, China; **Xuming Guo**, School of Materials Science and Engineering, Shenyang Aerospace University, Shenyang 110136, China; and **Zhenhua Li, Jing Ma, Fei Li,** and **Qingwei Jiang**, School of Materials Science and Engineering, Kunming University of Science and Technology, Kunming 650000, China. Contact e-mails: lifei06119@163.com and jqw6@163.com.

2. Wire Arc Additive Manufacturing (WAAM) Processes

WAAM is a rapid near-net-shaped process that employs arc to melt metal wire and produce components layer-by-layer along the designed path (Ref 18, 19). Depending on the nature of electrodes used, WAAM processes are generally divided into two types: non-consumable tungsten electrodes-based WAAM, such as gas tungsten arc welding wire arc additive manufacturing (Ref 20-22) (GTAW-WAAM) and plasma arc welding wire arc additive manufacturing (Ref 23, 24) (PAW-WAAM), and consumable electrode-based WAAM, such as gas metal arc welding wire arc additive manufacturing (Ref 25, 26) (GMAW-WAAM).

2.1 WAAM Processes Using Non-Consumable Tungsten Electrodes

Schematic diagrams of GTAW-WAAM and PAW-WAAM processes are illustrated in Fig. 1(a) and (b), respectively. These processes boast high arc stability and welding quality, albeit with comparatively low deposition efficiency as a result of the limited current-carrying capacity of the tungsten electrode (Ref 27, 28). Up to now, various series of aluminum alloy components can be produced using the GTAW-WAAM process (Ref 20, 29, 30). However, the restricted wire feeding angle limits the flexibility of the torch. To address this problem, Air Liquide (France) developed an advanced TOP-TIG process that allows for adjustable angles between the tungsten electrode and wire, ranging from 20 to 30 degrees. This special wire feeding mode alters the melting characteristics of the wire, increasing flexibility and efficiency (Ref 31, 32).

Multi-wire GTAW-WAAM process has been proven effective in increasing deposition efficiency by simultaneously feeding and melting multiple metal wires to fabricate components. Recent studies have confirmed its capability of additive manufacture of Al-Cu-Mg and Al-Zn-Mg-Cu alloy with poor weldability. Qi et al. (Ref 33), using the double-wire GTAW-WAAM process, successfully fabricated a series of Al-Cu-Mg alloy multilayer components (Al-3.6Cu-2.2 Mg, Al-4Cu-1.8 Mg, and Al-4.4Cu-1.5 Mg) that are less prone to cracking by matching ER2319 and ER5087 wires. They reported that the tensile strengths of these deposits both exceeded 280 MPa, however, the elongation had a decreasing trend from 8.2 to 6% with the increasing of Cu/Mg ratio. Yu et al. (Ref 34) used multi-wire WAAM process to fabricate Al-Zn-Mg-Cu alloy multilayer deposits by matching ER2319, ER5356, and pure zinc wires. The average hardness of the deposits was 106 HV, and the tensile strength was 241 MPa in the horizontal direction. Cong et al. (Ref 35) employed ultrasonic frequency pulsed variable polarity (UFPVP) TIG arc heat source to produce Al-4.57Cu-1.32 Mg alloy multilayer deposits by double-wire GTAW-WAAM. The application of ultrasonic frequency pulsed arc improved the arc stability and decreased defects during deposition. The WAAM Al-4.57Cu-1.32 Mg alloy exhibited the exceptional properties due to the refined grains and reduced porosity.

The PAW-WAAM process utilizes a plasma arc high energy density beam as a heat source to produce components, offering many advantages over GTAW-WAAM process such as higher energy density and arc stability, a small heat-affected zone, low weld distortion, and increased deposition efficiency (Ref 36, 37). The PAW-WAAM has been applied to produce multiple engineering alloys, such as Inconel 718, Ti6Al4V, and aluminum alloy (Ref 38-40). However, the research of Al-Cu alloy fabricated by PAW-WAAM is little.

2.2 WAAM Processes Using Consumable Electrodes

GMAW-WAAM, which uses the wire as electrode, has a deposition rate two–three times higher than that of GTAW-WAAM or PAW-WAAM process (Ref 41). The schematic diagram is shown in Fig. 2. However, it generates more weld fume and spatter due to low arc stability and causes the formation of coarse grains because of high heat input. The resulted in the invention of cold metal transfer (CMT), which enables a faster cooling rate and almost no spatter welding. CMT is a modified MIG welding process, including coordinated control of current magnitude and wire movement during short-circuiting transfer process (Ref 42-44). Zhou et al. (Ref 45) investigated the melt drop transfer behavior in both CMT and CMT + P modes. The melt drop transition transformed from short-circuit transition in CMT mode into the hybrid transition mode of short-circuit transition and globular transition in CMT + P mode. In the CMT mode, the formation of spatter was mainly attributed to the detachment of wire to bring out a small amount of metal liquid from the melt pool, while the spatter in CMT + P mode was mainly caused by the arc force and droplet free-fall motion. Additionally, compared with CMT

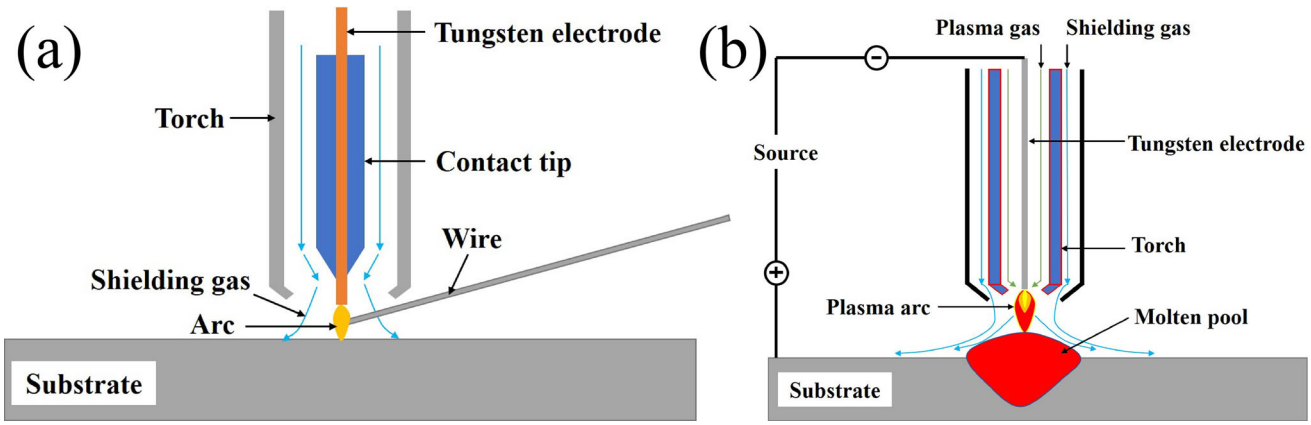

Fig. 1 Schematic representation of non-consumable tungsten electrodes-based WAAM: GTAW-WAAM and (b) PAW-WAAM

and CMT + P modes, CMT + A mode minimized the heat input and reduced porosity (Ref 46).

Similar to multi-wire GTAW-WAAM process, the multi-wire GMAW-WAAM process has also been developed. Gu et al. (Ref 47) produced a series of Al-Cu-Mg alloy components using a pulsed double-wire GMAW-WAAM process by combining various Al-Cu and Al-Mg wires. They reported that the Al-(4.2-6.3%) Cu-(0.8-1.5%) Mg alloys are less susceptible to cracks during deposition. In the Al-Cu-Mg system, the content of alloying elements is the key parameter depending on the cracking resistance. This is because different eutectic phase will generate during solidification when different content of Cu and Mg elements is added, causing the graded cracking susceptibility for Al-Cu-Mg alloy (Ref 47). In this range, solidification terminates in an isothermal eutectic reaction and the solidification pathway is dominated by the ternary eutectic reaction of $L \rightarrow \alpha\text{-Al} + \theta\text{-Al}_2\text{Cu} + \text{S-Al}_2\text{CuMg}$, and the minimum freezing range is located in this region. Fan et al. (Ref 48) reported that using ER2319 and ER5183 wires to manufacture crack-free Al-Cu-Mg alloy components by double-wire arc additive manufacturing process with CMT arc source is a viable option.

2.3 Hybrid Wire Arc Additive Manufacturing Processes

Investigations have been conducted on several hybrid WAAM processes for aluminum alloys, which combine different welding processes, such as laser-MIG hybrid additive manufacturing, double-electrode gas metal arc additive manufacturing and friction stir process (FSP) hybrid additive manufacturing (Ref 49). The diagrams of their respective schematics are illustrated in Fig. 3. These hybrid WAAM processes can improve forming quality without compromising deposition efficiency, thus being more suitable for industrial applications.

Zhang et al. (Ref 50) reported that the laser-MIG hybrid additive manufacturing process combined the advantages of laser welding and arc welding, allowing for high-precision and high-efficiency additive manufacturing due to the laser-arc synergy effects. Zhang et al. (Ref 51) investigated the effect of different laser power on the 2319 aluminum alloy specimens fabricated by the laser-MIG hybrid additive manufacturing. With the increase in laser power, the laser stirring effect on the molten pool was enhanced, thus refining the grain structures. When the laser power was 300 W, the grain structures consisted of equiaxed grains and the average size of grain was 30.8 μm. Liu et al. (Ref 52) used the double-electrode gas metal arc additive manufacturing process to produce 2219 aluminum alloy components. The bypass current ratio (a ratio of the currents, respectively, passing through the GMA torch and flowing into the GTA torch), which is a key factor for WAAMed alloys, determined the heat input during WAAM process. By changing the bypass current ratio, the tensile strength and elongation of WAAMed alloys in both the vertical direction and horizontal direction increased by 9.71 MPa, 18.89 MPa, 4.17%, and 5.74%, respectively. Wei et al. (Ref 53) demonstrated that the FSP hybrid additive manufacturing process had a considerable influence on minimizing porosity and refining microstructure. In a hybrid additive manufacturing process employing FSP, three layers were deposited using the same parameters, followed by milling of the top and side surfaces of the deposited materials with a milling machine with a thickness of 1.5 and 1 mm, respectively. Finally, the interlayer FSP was applied on the WAAMed deposits. The 2219 aluminum alloy thin wall of 300 mm in length, 12 mm in width, and 42 mm in height was successfully manufactured by repeating the above process (Ref 54). The FSP hybrid additive manufacturing process exhibits superior excellence on the microstructure refinement and porosity elimination of Al-Cu alloy. They reported that the average size of grains within the middle region stir zone was refined to 5.5 μm when the interlayer FSP process was applied, compared with 48 μm without the interlayer FSP process. Under the influence of interlayer FSP process, the eutectic structure in the as-deposited alloy was disrupted and dissolved into the α-Al matrix, leading to an increase in the supersaturation of the α-Al matrix. Subsequently, the effect of thermal cycle during WAAM led to the precipitation and coarsening of the θ' phase. Additionally, the interlayer FSP process also eliminated the porosity in the stir zone of the as-deposited alloy due to the severe plastic

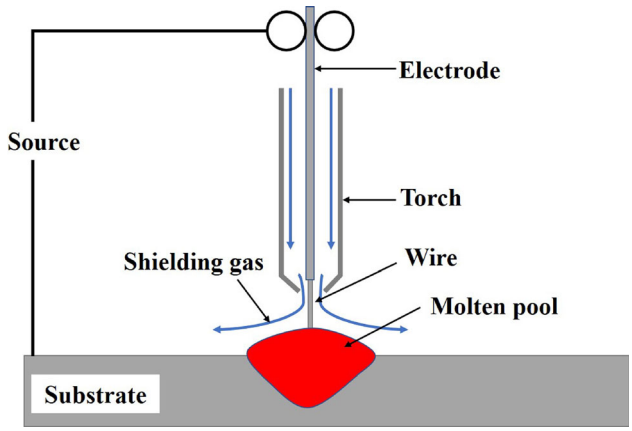

Fig. 2 Schematic representation of GMAW-WAAM

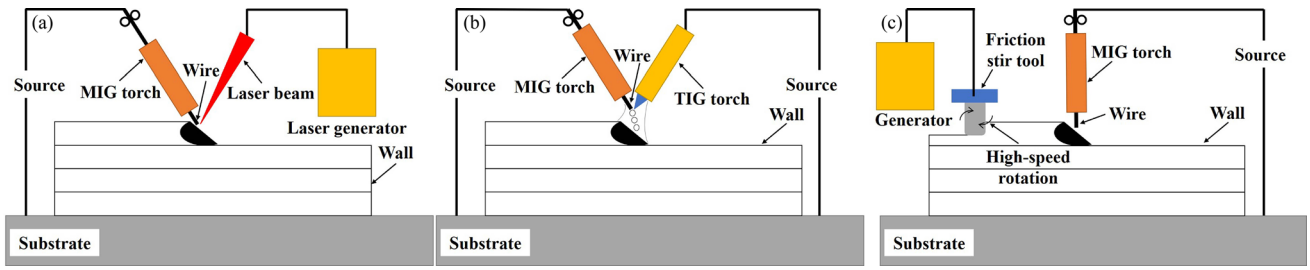

Fig. 3 (a) Laser-MIG hybrid additive manufacturing; (b) double-electrode gas metal arc additive manufacturing; and (c) friction stir process hybrid additive manufacturing

deformation introduced by the interlayer FSP process. They reported that no porosity defects were observed in OM and SEM images of the stir zone.

In addition to being combined with welding processes, there are several hybrid WAAM processes that combine WAAM process with cold working processes, such as interlayer rolling and interlayer hammering. Their effects can be described as follows: (1) eliminating metallurgical defects of WAAMed aluminum alloy; (2) minimizing the size of grain; and (3) improving the forming quality (surface roughness). These related contents are elaborated in Sect. 6.

3. Solidification Microstructure and its Influencing Factors of the WAAMed Al-Cu alloys

The mechanical properties and cracking resistance of WAAMed Al-Cu alloys are highly dependent on the solidification microstructure. This section reviews the solidification microstructure and second phase of WAAMed Al-Cu alloys. Additionally, the key process parameters in determining the solidification microstructure are discussed.

3.1 Solidification Grain Structures

The typical solidification grain structures of WAAMed Al-Cu alloys during various processes are shown in Fig. 4 (Ref 47, 55-57). A similar feature can be described as follows: (1) At lower deposition heights, there are fine equiaxed grains (FQZ) in the interlayer zone and columnar grains in the innerlayer zone and (2) at higher deposition heights, the interlayer zone contains FQZ, while the innerlayer zone consists of columnar grains and coarse equiaxed grains. These heterogeneous band characteristics between interlayer zone and innerlayer zone are related to the change in the heat dissipation and heat accumulation dominated by the thermal cycles during WAAM process.

Bai et al. (Ref 58) reported that the thermal cycles during deposition can be classified into three categories: the melting heat, partial-melting heat, and post-heat. In a single deposition layer, the melting heat influenced the microstructure of the top region, the microstructure of the line between the top and bottom regions (the partial-melting-affected zone) resulted from the melting heat and partial-melting heat, and all three thermal cycles cooperated to form the microstructure of the bottom region. Wang et al. (Ref 55) conducted a systematic study on the solidification grain structures of WAAMed 2219 Al-Cu alloy. For the WAAMed materials, the shape and size of the

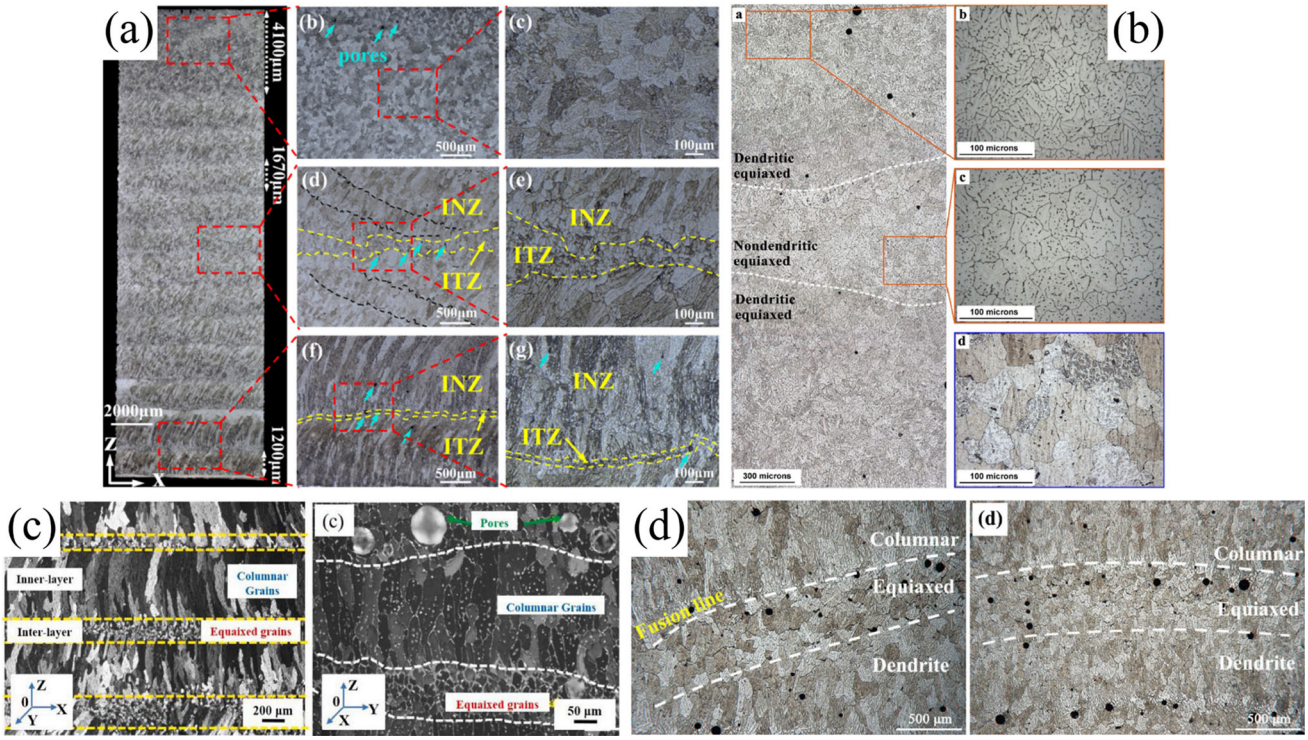

Fig. 4 Grain structures of WAAMed Al-Cu alloys: (a) 2219 alloy fabricated by CMT-WAAM [55]; (b) Al-4.3Cu-1.5 Mg alloy fabricated by CMT-WAAM [56]; (c) 2219 alloy fabricated by GTAW-WAAM [57]; and (d) Al-5.5Cu-2.2 Mg alloy fabricated by double GWAM-WAAM [47]. Panel (a) reprinted from *Additive Manufacturing,* Vol 47, Zhennan Wang, Xin Lin, Lilin Wang, Yang Cao, Yinghui Zhou, Weidong Huang, Microstructure evolution and mechanical properties of the wire + arc additive manufacturing Al-Cu alloy, Article 102,298, Copyright 2021, with permission from Elsevier. Panel (b) reprinted from *Materials and Design*, Vol 186, J. Gu, M. Gao, S. Yang, J. Bai, Y. Zhai, J. Ding, Microstructure, defects, and mechanical properties of wire + arc additively manufactured Al Cu4.3-Mg1.5 alloy, Article 108,357, Copyright 2020, with permission from Elsevier. Panel (c) reprinted from *Journal of Alloys and Compounds,* Vol 865, Y. Zhou, X. Lin, N. Kang, Z. Wang, H. Tan, W. Huang, Hot deformation induced microstructural evolution in local-heterogeneous wire + arc additive manufactured 2219 Al alloy, Article 158,949, Copyright 2021, with permission from Elsevier. Panel (d) reprinted from *Journal of Materials Processing Technology,* Vol 262, J. Gu, J. Bai, J. Ding, S. Williams, L. Wang, K. Liu, Design and cracking susceptibility of additively manufactured Al-Cu-Mg alloys with tandem wires and pulsed arc, Pages 210–220, Copyright 2018, with permission from Elsevier

molten pool had a major influence on the morphology and dimensions of the solidification microstructure (Ref 59, 60). According to the discussion of Wang et al. (Ref 55), the angle γ was defined as the angle between the normal directions of the adjacent molten pool boundaries, as shown in Fig. 5 (Ref 55). When the deposition height was low, the cold substrate caused a fast cooling rate, which led to a shallow molten poor (with a small γ), as shown in Fig. 5(a). At this time, the direction of temperature gradient was nearly perpendicular to the substrate and parallel to the building direction. Thus, the α-Al grains in the new molten pool grew epitaxially into longer columnar grains along the building direction. With the increase in deposition height, the increased heat accumulation of the deposits resulted in a slower heat dissipation and lower cooling rate (Ref 61, 62). Therefore, the angle γ increased as the molten pool deepened, as shown in Fig. 5(b). Considering the change in the direction of the temperature gradient, the dendrites with the same direction as the temperature gradient were the easiest to dominate during solidification, resulting in directionally growth in the new molten pool (Ref 63).Furthermore, with the increasing heat accumulation, the continuously slowing heat dissipation led to a small difference in the temperature gradient, approaching a thermal balance (Ref 56). The α-Al grains in the new molten pool were nucleated based on existing nucleation nuclei and grew spatially with the similar speed in each direction, thereby developing coarse equiaxed grains (Ref 48, 56). These studies adequately explained the formation of columnar grains zone and coarse equiaxed grains zone.

According to the classical solidification theory, the relationship between the temperature gradient $\boldsymbol{G}$, the dendrite tip undercooling $\boldsymbol{\Delta T}$ and the volume fraction of equiaxed grains $\boldsymbol{\varphi}$ can be expressed as (Ref 64):

$$G = \frac{1}{\mathrm{m}+1} \times \sqrt[3]{\frac{-4\pi}{3\ln[1-\varphi]}} \times N_0^{1/3} \times \Delta T \times \left(1 - \frac{\Delta T_n^{\mathrm{m}+1}}{\Delta T^{\mathrm{m}+1}}\right) \quad \text{(Eq 1)}$$

Wang et al. (Ref 55) simplified Eq. 1 to:

$$\frac{G^m}{V} = a\left\{\sqrt[3]{\frac{-4\pi N_0}{3\ln(1-\varphi)}} \times \frac{1}{1+m}\right\}^m \quad \text{(Eq 2)}$$

where $\boldsymbol{a}$ and $\boldsymbol{m}$ are constants related to the nature of materials, $\boldsymbol{V}$ is the solidification velocity of the columnar front, and $\boldsymbol{N_0}$ is the nuclei density.

According to Eq. 2, Wang et al. (Ref 55) discussed that the optimal solidification condition for forming equiaxed grains is high $\boldsymbol{V}$ and low $\boldsymbol{G}$, whereas high $\boldsymbol{G}$ and low $\boldsymbol{V}$ favor the formation of columnar grains. It is well known that high $\boldsymbol{G}$ and

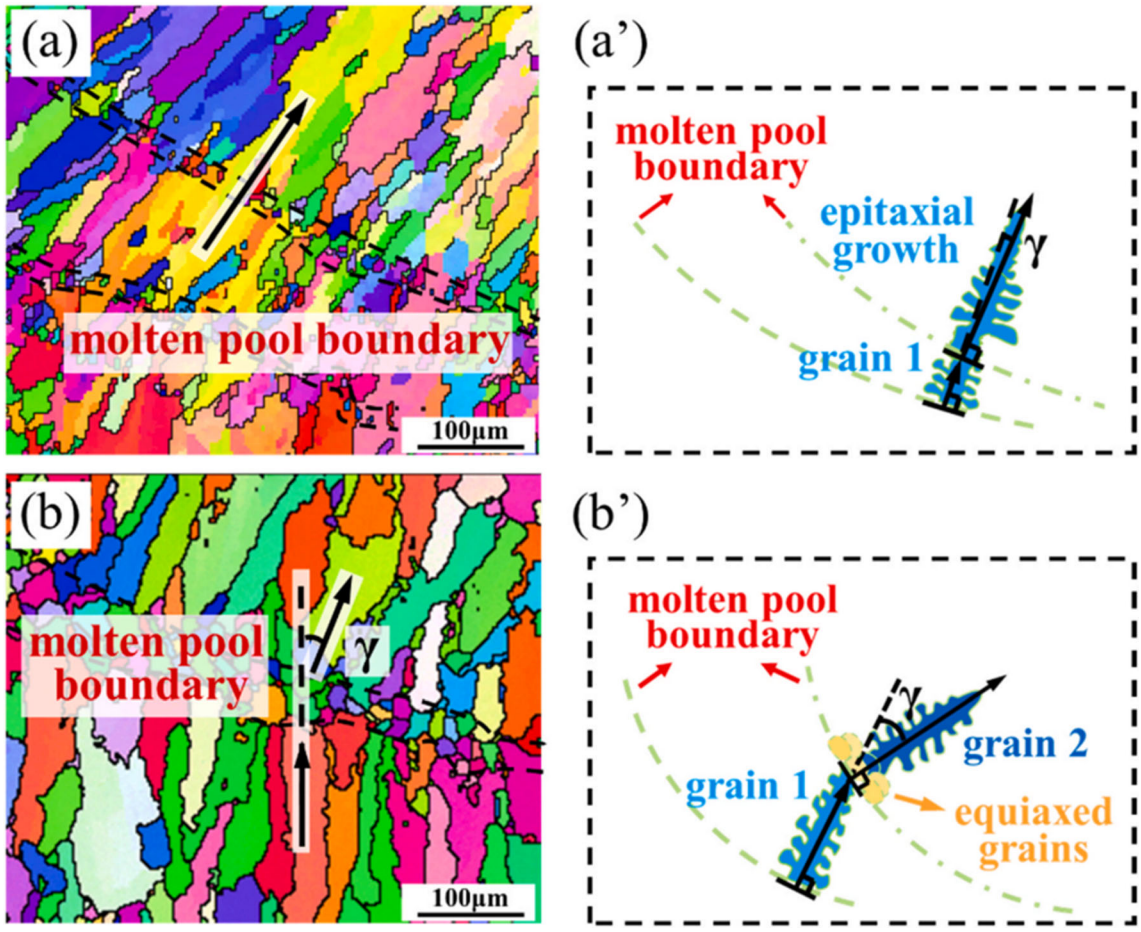

Fig. 5 The EBSD maps (a) the bottom region and (b) the middle region, and the corresponding schematic diagrams of their dendrites growth orientation. γ: The angle between the normal directions of the adjacent molten pool boundaries [55]. Reprinted from *Additive Manufacturing,* Vol 47, Zhennan Wang, Xin Lin, Lilin Wang, Yang Cao, Yinghui Zhou, Weidong Huang, Microstructure evolution and mechanical properties of the wire + arc additive manufacturing Al-Cu alloy, Article 102,298, Copyright 2021, with permission from Elsevier

low V typically occur at the bottom of the molten pool. However, FQZs are usually observed in the solidification microstructure of WAAMed Al-Cu alloys at the bottom of molten pool. Wang et al. (Ref 55) speculated that the formation of FQZs was due to the heterogeneous nuclei of Al_3Zr precipitates which formed in the molten pool. The primary Al_3Zr phase precipitated at temperatures between 1016.02 K to 915.69 K which provided the high nuclei density N_0 that overcame the effect of G/V, thus enabling the formation of FQZs even when G/V was large. Hu et al. (Ref 65) reported that the formation of FQZs was observed in melting welding-based Al-Li and Zr-containing aluminum alloys due to the heterogeneous nucleation of $Al_3(Li_x, Zr_{1-x})$ and Al_3Zr, respectively. Due to the plastic incompatibility between the hard phases and soft (low precipitate density) grain interiors in the FQZ, cracking occurred in a FQZ of aluminum alloys.

In summary, the distinctive thermal cycles of WAAM process dominate the transformation from columnar grains to equiaxed grains, while the heterogeneous nucleation of Al_3Zr precipitates promotes the formation of FQZs at the bottom of molten pool. The FQZs should be eliminated since it increases the chance of cracks occurring.

3.2 Second Phase

Cu and Mg, as the main strengthening alloying elements, were added into pure aluminum to form Al-Cu-(Mn) alloy (the content of Cu typically range from 5.8 to 6.8 wt.%, and that of Mn is from 0.2 to 0.5 wt.%) and Al-Cu-Mg alloy (the content of Cu typically ranges from 3.8 to 4.9 wt.%, corresponding to the content of Mg of 1.2-1.8 wt.%), respectively. There are three existence forms of Cu and Mg elements in WAAMed Al-Cu alloys, as follows:

(1) Solute atoms: Cu and Mg elements are generally dissolved into the α-Al matrix through substitutional solid solution, due to their large solid solubility, thus contributing to the solid solution strengthening.
(2) Second phases: Since the reaction of Cu and Mg with Al belongs to the eutectic reaction and the equilibrium segregation coefficient $K_0 < 1$, the excess Cu and Mg solute atoms tend to be repelled to the dendrite boundaries by solidified solid phases and react with Al to form eutectic structures during solidification. The formation of eutectic structures reduces the content of Cu and Mg solute atoms available for aging precipitation, thus weakening the precipitation strengthening. On the other hand, the existence of the low melting point eutectic structures increases the possibility of the formation of cracks. Therefore, the formation of eutectic structures should be minimized as much as possible during WAAM.
(3) Secondary phases: The aging treatment homogeneously precipitates Cu and Mg elements from the α-Al matrix to form secondary phases, with a good coherent interface between the α-Al matrix and the secondary phases being the key to precipitation strengthening (Ref 66). However, the coherent interface will be lost with the increase in aging time. Thus, the aging treatment must be carefully managed to prevent secondary phases from transforming into the equilibrium phases.

Figure 6 shows the SEM images of the second phase for the WAAMed Al-Cu alloys. Gu et al. (Ref 67) reported that the white network-like θ-Al_2Cu phases were scattered along the grain boundaries or distributed in the intra-grain regions, as shown in Fig. 6(a). Similarly, Zhou et al. (Ref 68) reported that the white θ-Al_2Cu second phases present in the WAAMed Al-Cu alloy were eutectic structures of α-Al + θ-Al_2Cu, distributed continuously along the grain boundaries or dendrite boundaries. Qi et al. (Ref 33) reported that the second phases in the WAAMed Al-4.4Cu-1.5 Mg alloys were α-Al, θ-Al_2Cu, and S-Al_2CuMg, which were net-likely distributed along the grain boundaries or scattered inside the grains, as shown in Fig. 6(b). The eutectic structures typically exhibited the distributions of long strip-like or skeletal-like along the grain boundaries (Ref 48). Zhou et al. (Ref 69) reported that the secondary phases θ' precipitated from the α-Al matrix due to the effect of thermal cycles during WAAM, as shown in Fig. 7. With the increase in the number of thermal cycles, the precipitation density of secondary phases θ' was increased. Xu et al. (Ref 70) indicated that the thermal cycles resulted in an increasing of heat accumulation for the already deposited components, thereby partially remelting the previously deposition layer with a peak temperature above 700 °C, promoting the precipitation of secondary phases in the already deposited alloys. Wang et al.(Ref 71) pointed out that the secondary phases θ' were not found in the 2219 aluminum alloys fabricated by traditional cast and wrought processes. The thermal cycles induced the precipitation of secondary phases θ' during depositions, decreasing the supersaturation of Cu solute atoms in the α-Al matrix, which decreased the precipitation strengthening (Ref 69).

In summary, the main second phases of Al-Cu-(Mn) alloys were α-Al and θ-Al_2Cu, while those of Al-Cu-Mg alloys were α-Al, θ-Al_2Cu, and S-Al_2CuMg. The distinctive thermal cycles of the WAAM process were equivalent to a short aging treatment for the already deposited alloys, leading to the precipitation of the secondary phases from the α-Al matrix. In addition to θ-Al_2Cu and S-Al_2CuMg phases, T-Al(Cu, Mn), Al_3Ti, Al_3Zr, and impurity phases associated with Fe and Si were commonly observed in the WAAMed Al-Cu alloys. These relevant contents are discussed in Sect. 3.4.

3.3 Effect of Heat Input

Heat input is a decisive process variant that decides the deposition geometry, microstructure evolution, defect formation, and mechanical properties during WAAM (Ref 72, 73). The relation between heat input (HI) and welding process parameters can be expressed as:

$$\mathrm{HI} = \frac{\eta \mathrm{UI}}{V} \quad \text{(Eq 3)}$$

where I and U are the welding current and voltage, respectively, V is the welding velocity, and η is the thermal efficiency of heat source.

Zhou et al. (Ref 68) used the AC-TIG WAAM process to fabricate 2219 alloys with the wire feed speed of 2 m/min and the current intensity of 150 A. When the welding velocity increased from 150 to 350 mm/min in units of 100 mm, the tensile properties of the 2219 alloys increased trend from 216.7 to 273.5 MPa. However, the tensile strength decreased to 259.6 MPa when the welding velocity was increased to 450 mm/min. The reduction in tensile strength at 450 mm/min was attributed to the fact that the segregation of copper atoms in the large number of dendrites and grain boundaries,

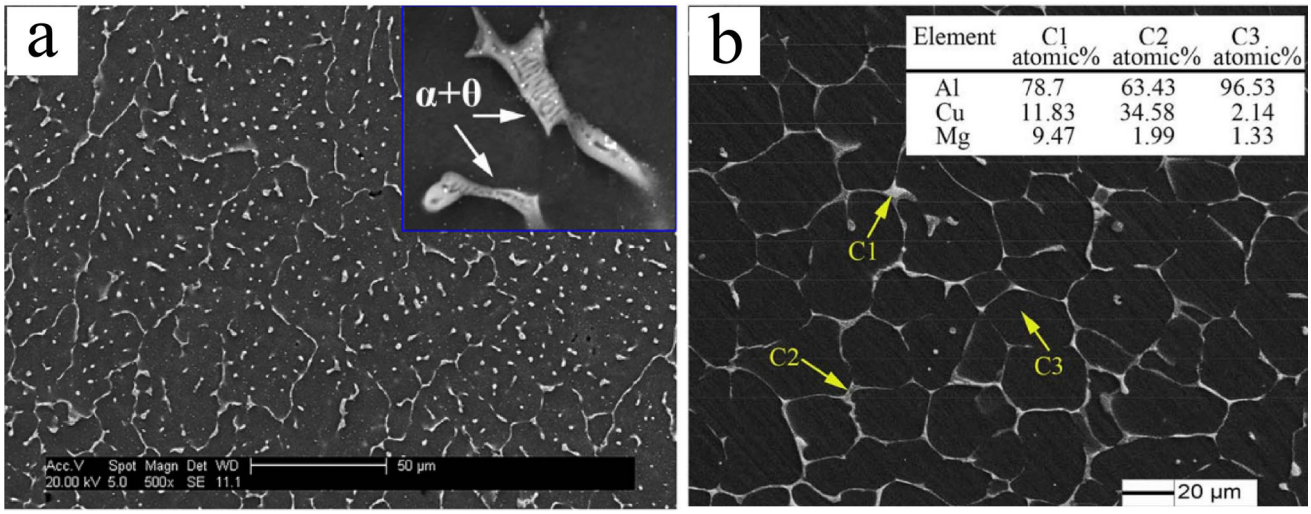

Fig. 6 The SEM images of second phase for the WAAMed Al-Cu alloys: (a) 2319 Al-Cu alloy [67] and (b) Al-4.4Cu-1.5 Mg alloy [33]. Panel (a) reprinted from *Materials Science and Engineering: A,* Vol 651, J. Gu, J. Ding, S.W. Williams, H. Gu, J. Bai, Y. Zhai, P. Ma, The strengthening effect of inter-layer cold working and post-deposition heat treatment on the additively manufactured Al–6.3Cu alloy, Pages 18–26, Copyright 2016, with permission from Elsevier. Panel (b) reprinted from *Journal of Materials Processing Technology,* Vol 255, Z. Qi, B. Cong, B. Qi, H. Sun, G. Zhao, J. Ding, Microstructure and mechanical properties of double-wire + arc additively manufactured Al-Cu-Mg alloys, Pages 347–353, Copyright 2018, with permission from Elsevier

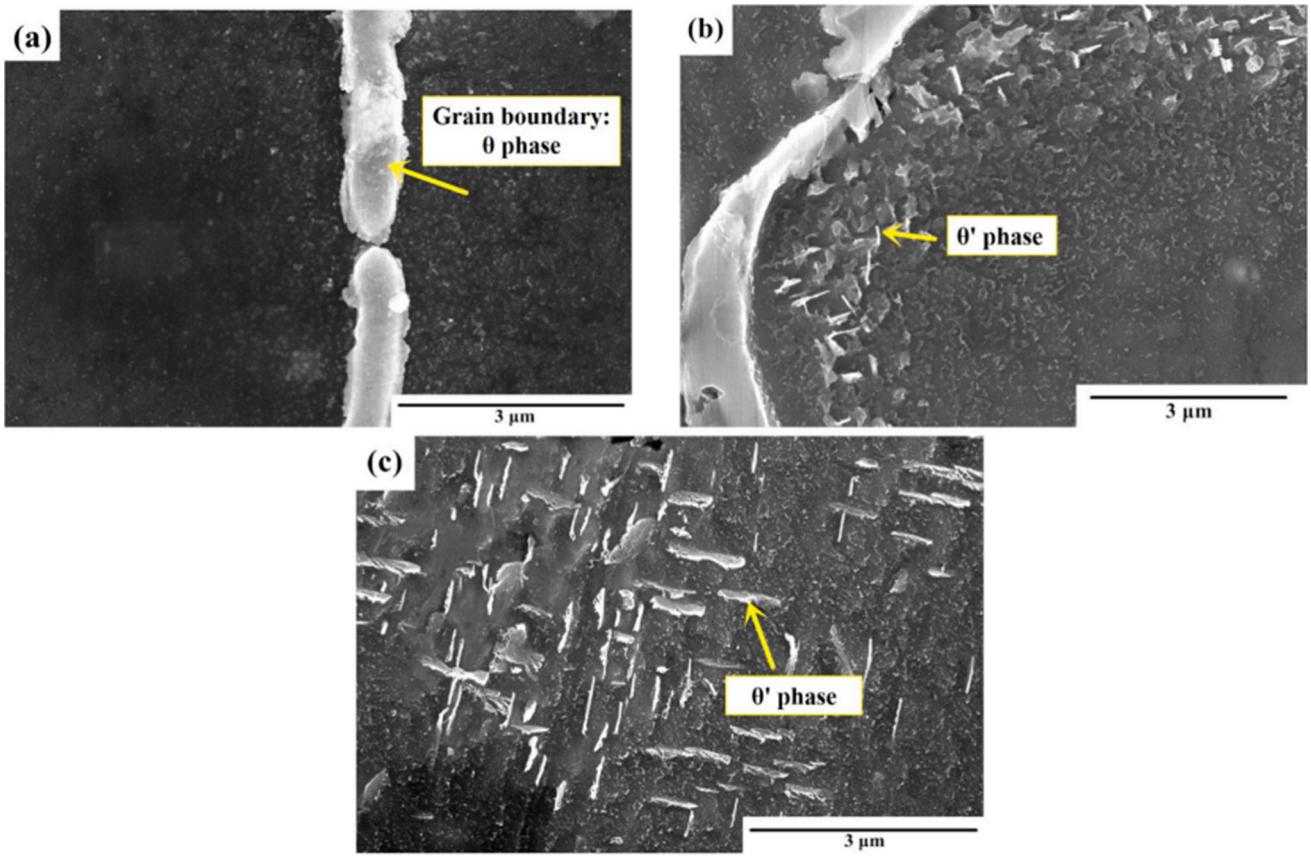

Fig. 7 The microstructure for the WAAMed 2219 Al alloy [69]: (a) the upper parts; (b) the center parts; (c) the bottom parts. Reprinted from *Materials Characterization,* Vol 171, Y. Zhou, X. Lin, N. Kang, W. Huang, Z. Wang, Mechanical properties and precipitation behavior of the heat-treated wire + arc additively manufactured 2219 aluminum alloy, Article 110,735, Copyright 2021, with permission from Elsevier

forming numerous θ phase precipitates which reduced the remaining Cu atoms and the volume fraction of θ'' phase during depositions. When the welding velocity was 350 mm/min, a small amount of θ' phase and a large amount of θ'' phase near the grain boundary without θ phase can be observed. This is the reason why the highest tensile strength was obtained

when the welding velocity was 350 mm/min. Wang et al. (Ref 74) reported that the lower heat input was beneficial for manufacturing components of high forming quality, avoiding the overflow and collapse of the molten pool and reducing the residual stresses. Cong et al. (Ref 46) investigated the effect of different CMT mode (CMT + P and CMT + A) on the microstructure and mechanical properties of 2319 alloys fabricated by CMT-WAAM process. The CMT + A process yielded the minimum heat input, while the heat input of CMT + P process was larger. Although both the columnar grains and equiaxed grains were found in 2319 alloys fabricated by the two processes, the micro-hardness of specimens fabricated by CMT + A process was higher due to the lower heat input which reduced the porosity. Xiong et al. (Ref 75) reported that decreasing the interlayer temperature was associated with the improvement in surface quality of thin-wall components with other parameters being kept constant. A lower wire feeding velocity matching a lower welding velocity could reduce the surface roughness.

The various welding process variants such as current, voltage, wire feeding velocity, welding velocity, and arc mode collectively affect the heat input during WAAM (Ref 76, 77). However, WAAM is associated with the multilayer deposition and inhomogeneous thermal cycles. The effect of heat input can be understood as follows: (1) Processing at high heat input conditions accelerates the heat accumulation, formation of coarse grains, increased residual stresses, and decreased mechanical properties. Nevertheless, the molten pool collapse possibly occurs at very high heat input conditions. (2) Processing at low heat input conditions is beneficial for the formation of fine grain, porosity reduction, and residual stress minimization, countering the issues mentioned above associated with high heat input conditions. Therefore, the suitable heat input conditions should be employed during WAAM.

3.4 Effect of Alloying Elements

The micro-alloying elements such as Mg, Mn, Ti, Zr, Cd, Sn, and Ag are added into the Al-Cu alloy wires in order to improve the microstructure and mechanical properties of the deposits. On the other hand, Fe and Si are generally considered as impurity elements in the Al-Cu alloy wires, which come from the impure master alloys during melting process. Table 1 lists the Al-Cu alloy wires that have been used for WAAM. In this section, the effects of these micro-alloying elements added into the Al-Cu alloy wires on the microstructure and mechanical properties of Al-Cu alloy deposits are discussed.

(1) Cu and Mg: Cu and Mg elements are added into the Al-Cu alloys to provide the solid solution strengthening and precipitation strengthening. However, if too much Cu and Mg are added, they can react with Al to form lots of eutectic structures, which would negatively impact the mechanical properties of the deposits and increase the cracking sensitivity. Therefore, the content of Cu and Mg added into the currently applied Al-Cu alloy wires is usually kept lower than their ultimate solid solution degree in the aluminum. Al-Cu-Mg alloys have higher tensile strength than Al-Cu-Mn alloys at the room temperature. But the addition of Mg reduces the solubility of Cu in the Al-Cu alloys and increases the brittle temperature range since the low melting point eutectic S-Al_2CuMg phases are precipitated along the grain boundaries (Ref 78-80). This makes Al-Cu-Mg alloys more prone to cracking and there are currently limited Al-Cu-Mg alloy wires that can be applied to WAAM process.

(2) Mn: The addition of Mn improves the heat resistance and reduces the crack sensitivity of WAAMed Al-Cu alloys. However, an excessive amount of Mn can promote the formation of T-$Al_{13}Cu_4Mn_3$ phase, which is beneficial to enhance the heat resistance of the alloys but also consumes a part of Cu atoms, and T-$Al_{13}Cu_4Mn_3$ phase is nearly insoluble at high temperatures, thus reducing the precipitation strengthening of Al-Cu alloys (Ref 81). Therefore, the content of Mn added into the Al-Cu alloy wires should not be too high in general.

(3) Ti and Zr: Ti and Zr elements are added into the Al-Cu alloy wires as the grain refiners. The Al_3Ti and Al_3Zr phases formed by the reaction of Ti and Zr with Al, respectively, are similar to the α-Al phases in both crystal structure and lattice constant. As a result of the low mismatch with Al, these particle phases can act as the heterogeneous nucleation nuclei of α-Al, refining the grain structures, according to the principle of coherent interface (Ref 82, 83). Zhou et al. (Ref 84) used a special 205A alloy wire containing 0.28 wt.% Ti and 0.16 wt.% Zr to deposit Al-Cu alloy thin-wall components by CMT-WAAM process. The grain structures consisted of a large number of fine equiaxed grains because of the heterogeneous nucleation nuclei of Al_3Ti and Al_3Zr phases.

(4) Cd, Sn, and Ag: Zhou et al. (Ref 84) reported that due to the lower activation energy than Cu atoms, the Cd atoms, vacancies, and Cu atoms formed Cu-Cd-vacancy clusters during aging treatment process. The formation of these clusters promoted the precipitation of θ' phases, which significantly improved the mechanical properties of the deposits. Dong et al. (Ref 85) proposed a se-

Table 1 Chemical composition of Al-Cu wires used in WAAM

Wires	Compositions, wt.%								
	Cu	Mg	Mn	Ti	Zr	Cd	Sn	Ag	Al
2219-Al (Ref 20)	5.8–6.8	…	0.2–0.4	0.1–0.2	0.1–0.25	…	…	…	Bal
2319-Al (Ref 111)	5.8–6.8	…	0.2–0.4	0.1–0.2	0.1–0.25	…	…	…	Bal
2139-Al (Ref 87)	4.7	0.52	0.36	0.051	…	…	…	0.38	Bal
205A-Al (Ref 84)	5.15	…	0.42	0.28	0.16	0.22	…	…	Bal
Al-Cu-Sn (Ref 86)	5.1	0.025	0.042	0.27	0.177	…	0.1	…	Bal
Al-4.3Cu-1.5 Mg (Ref 56)	4.36	1.57	0.67	0.15	0.16	…	…	…	Bal

quence of aging process for Al-Cu-Cd alloys, which includes SSS (supersaturated solid solution) → Cd-vacancy cluster → θ' phase → θ phase. According to the strengthening model, adding Cd to ER2319 wires increased the yield strength by 43 MPa in the building direction of the heat-treated Al-Cu alloy wall components. Although Cd significantly improves the strengths of heat-treated Al-Cu alloys fabricated by WAAM, it is toxic and pollutes the environment during production. As an alternative, Wang et al. (Ref 86) developed the Al-Cu-Sn alloy wires by replacing Cd with non-toxic Sn. The Al-Cu-Sn thin-wall components were deposited by CMT-WAAM process. They reported that the Sn promoted the precipitation of θ' phases and the strength of WAAMed Al-Cu-Sn alloys was significantly increased after heat treatment. Brice et al. (Ref 87), using ER2139 alloy wires, deposited Al-Cu-Mg-Ag alloys and investigated the effect of Ag. They reported that the combined addition of Cu, Mg, and Ag promoted the formation of Ω-Al_2Cu phases and refined the sizes and distributions of Ω-Al_2Cu phases, thus enhancing the precipitation strengthening.

In conclusion, the type and content of alloying elements have a significant impact on the microstructure and mechanical properties of WAAMed Al-Cu alloys. However, further research is required, as there is still limited information available regarding the types of wires used in WAAM processes. Moreover, element loss during WAAM must be considered. Thus, it is essential to optimize the composition of the wires and develop specific Al-Cu alloy wires for WAAM processes.

4. Common Defects in the WAAMed Al-Cu Alloys

Al-Cu alloy components fabricated by WAAM exhibit good mechanical properties typically; however, there are some defects that hinder their applications. These defects can be divided into two categories: process-related defects, such as inhomogeneous microstructure, porosity, residual stress, and distortion, and material-related defects, such as inhomogeneous microstructure, porosity, and solidification cracks.

4.1 Inhomogeneous Microstructure

As discussed in Sects. 3.1 and 3.2, the deposits undergo inhomogeneous thermal cycles during WAAM, resulting in an inhomogeneous microstructure. The level of inhomogeneity is determined by the nature of the thermal cycles (Ref 88). Reasons for the formation of inhomogeneous grain structures are discussed in Sect. 3.1. On the other hand, the inhomogeneous microstructure is also reflected in the segregation of alloying elements.

Geng et al. (Ref 89) indicated that the molten pool during WAAM is smaller than that of the casting process, so the macroscopic segregation is unlikely to occur. However, the high cooling rate of the WAAM process leads to the insufficient time for solute atoms to diffuse, resulting in the micro-segregation appearing between dendrites and even cracking in the solidification microstructure. Gu et al. (Ref 56) deposited Al-Cu-Mg alloys by CMT-WAAM process, which showed obvious micro-segregation between dendrite boundaries, especially for Cu elements, as shown in Fig. 8.

Recent studies have shown that using the interlayer rolling process can refine the microstructure and reduce segregation. Gu et al. (Ref 67) applied the interlayer rolling process to treat WAAMed Al-Cu alloys. They reported that many eutectic structures were broken into small pieces during interlayer rolling process, indicating that the interlayer rolling process reduced the degree of microstructural segregation. Jin et al. (Ref 90) fabricated the TiC-reinforced 2219 alloy thin-wall components by GTAW-WAAM process. TiC particles, with a lower value of the nucleation supercooling, providing multi-site heterogeneous nucleation and significantly inhibited the constitutional supercooling caused by the segregation of Cu, thus weakening the degree of grain boundary segregation. Gu et al. (Ref 67) reported that the eutectic structures of α-Al + θ-Al_2Cu in the WAAMed 2219 alloys were dissolved during the solution treatment process, and then, the secondary phases were uniformly precipitated from the α-Al matrix during subsequent aging treatment process. The segregation of Cu solute atoms was significantly improved. However, due to the insufficient dissolution under the T6 heat treatment condition, a small amount of the eutectic structures of α-Al + θ-Al_2Cu still remained.

As a result of non-equilibrium solidification, the inhomogeneous microstructure seems to be inevitable during WAAM. Fortunately, it can be improved through the use of low heat input deposition processes, coating of TiC particle, optimization of wires, and post-processing processes such as interlayer rolling and heat treatment processes.

4.2 Porosity

Porosity is the most common defect in the melt welding-based Al-Cu alloys. The shape, size, and number of pores significantly affect the mechanical properties of Al-Cu alloys fabricated by WAAM. It is necessary to minimize or inhibit the pore formation to improve the density of deposits. Generally, the formations of pores in Al-Cu alloys can be divided into the endogenous pores and exogenous pores. Endogenous pores are formed when gases dissolved in liquid metals at high temperatures are trapped by the solidified metal due to the sudden decrease in solubility during solidification and phase transition processes, such as hydrogen and nitrogen. Exogenous pores are formed when contaminants from the air, wires, or substrates intrude into the molten pool to form pores.

Hauser et al. (Ref 91) reported that there are three main causes of porosity in the WAAMed aluminum alloys: (1) porosity induced by ambient gas; (2) shielding gas influence on the molten pool; and (3) porosity of gas bubble escape. Increasing the shielding gas flow rate tended to promote the formation of porosity in the WAAMed aluminum alloys, as the faster solidification of the molten pool caused by increased convective cooling prevented the escape of gases, as shown in Fig. 9. Ryan et al. (Ref 92) investigated the effects of different CMT modes, welding parameters, and wire quality on the porosity of WAAMed 2319 alloys. The surface finish of the wires was found to be a major factor in the porosity of WAAMed alloys, whereas porosity was not strongly dependent on CMT modes and welding parameters. The surface finish affected the amount of hydrogen on the wire surface and arc stability and subsequently affected the porosity during WAAM. Derekar et al. (Ref 93) investigated the effects of pulsed

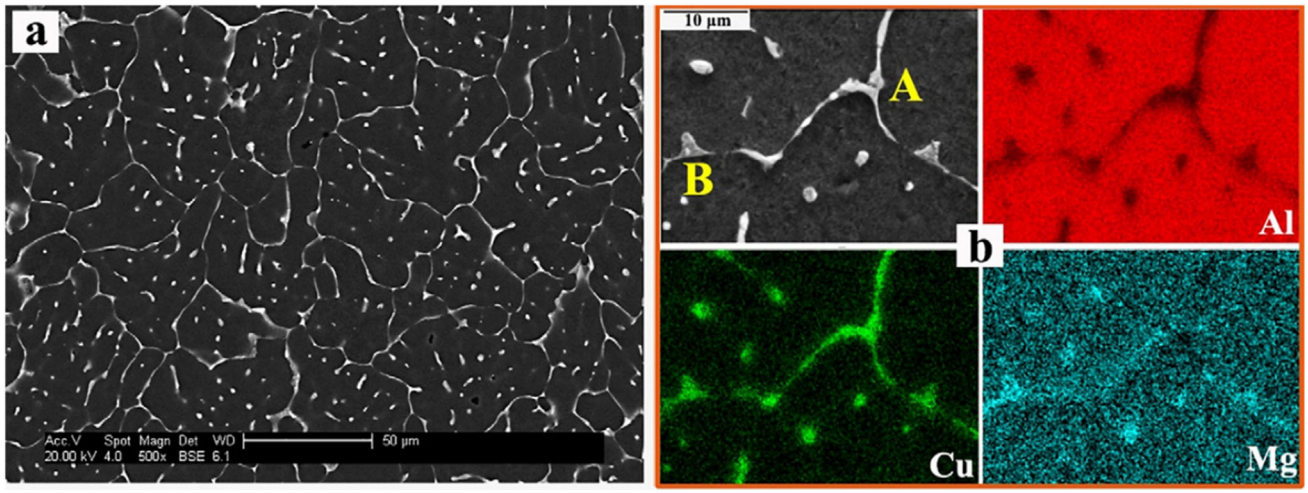

Fig. 8 SEM images of WAAM Al-4.3Cu-1.5 Mg alloy: (a) as-deposited and (b) map scanning of elements [56]. Reprinted from *Materials and Design,* Vol 186, J. Gu, M. Gao, S. Yang, J. Bai, Y. Zhai, J. Ding, Microstructure, defects, and mechanical properties of wire + arc additively manufactured Al Cu4.3-Mg1.5 alloy, Article 108,357, Copyright 2020, with permission from Elsevier

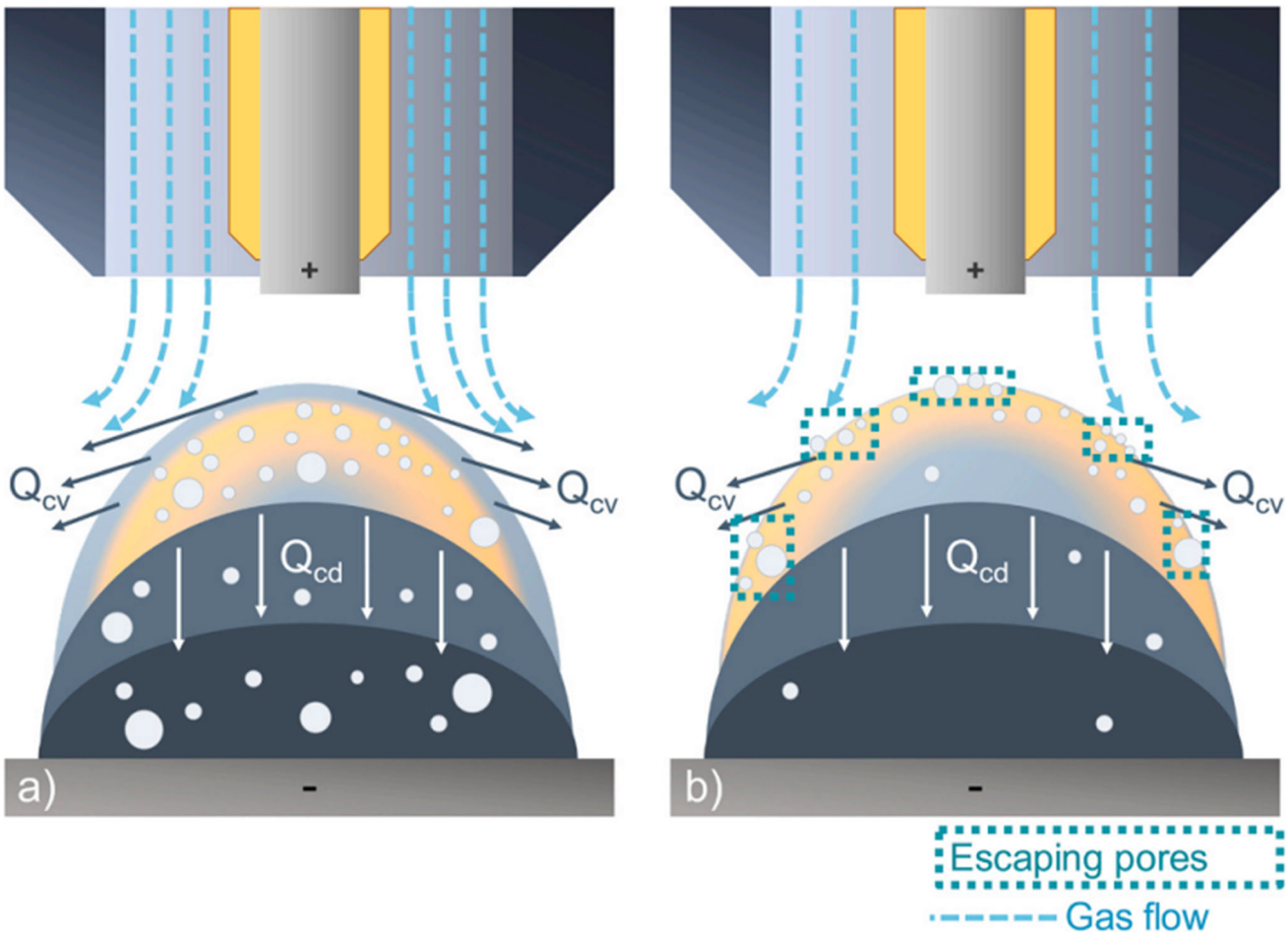

Fig. 9 Sketch of the cross section showing the influence of the gas flow rate on solidification and pore behavior of the layer for [91] (a) higher gas flow rates and (b) lower gas flow rates. Reproduced from *Additive Manufacturing,* Porosity in wire arc additive manufacturing of aluminium alloys, by T. Hauser et al. under the CC BY license

GMAW-WAAM and CMT-WAAM processes on the hydrogen dissolution in the WAAMed aluminum alloys. The samples produced by pulsed GMAW-WAAM process absorbed more hydrogen compared to samples deposited with CMT-WAAM process. Accordingly, the pulsed GMAW-WAAMed samples had higher number and volume fractions of porosity. In

comparison, the CMT-WAAM process dissolved more hydrogen due to its lower arc energy and heat input. Gu et al. (Ref 94) investigated the pore formation and evolution of WAAMed 2319 alloy thin-wall components. They reported that different amounts and morphologies of hydrogen micropores and solidification microvoids were observed in the as-deposited alloys due to the inhomogeneous microstructure and second phases distribution in each section of deposits, as shown in Fig. 10(a-c). Moreover, the deterioration of pore defects was significantly observed during heat treatment process (Fig. 10d-f), which was attributed to the combined effect of the hydrogen micropore precipitation, phases particle dissolution, and micropore growth. Similarly, Wang et al. (Ref 95) also reported that the porosity density was increased in the WAAMed 2319 alloys after heat treatment process. The hydrogen micropore precipitation was the key reason for the formation of new pores during heat treatment process. Gu et al. (Ref 96) employed the interlayer rolling process with a rolling road of 45 kN to deposit 2319 alloy components by CMT-WAAM process. Key findings demonstrated that the pores larger than 5 μm in diameter in the as-deposited alloys were eliminated. Therefore, no pores larger than 5 μm in diameter were observed in the samples after post-rolling heat treatment even though the areas of the pores increased during heat treatment process.

In summary, in order to reduce porosity, the following measures can be taken: (1) using low heat input WAAM processes; (2) selecting wires with the best surface finish; (3) increasing the purity of the shielding gas and adjusting the flow rate; (4) cleaning the wires and substrates before deposition; and (5) employing the interlayer cold working, such as interlayer rolling process.

4.3 Solidification Crack

Solidification cracks are the typical metallurgical defects in the Al-Cu alloys fabricated by WAAM. It is well established that the metal that crystallizes first is generally purer, while the metal crystallizing later contains more impurities which are enriched at the grain boundaries during crystallization. These impurities often form the eutectic phases with a low melting point. During the later stages of the metal solidification, the low melting point eutectic phases are exclusion to the dendrite boundaries by solidified solid phases, forming the ''liquid film,'' which is subject to the tensile stress due to the shrinkage of the weld. This ''liquid film'' becomes the weak zone, which is prone to cracking under the action of the tensile stress, forming the cracks. Al-Cu alloys belong to the eutectic alloys, and the formation of low melting point eutectic structures widens the brittle temperature range of the Al-Cu alloys, thus increasing the susceptibility to solidification cracking (Ref 48).

Ouyang et al. (Ref 29) reported that the susceptibility to solidification cracking of WAAMed aluminum alloys was exacerbated by the coarse grain structures and second phase segregation along the grain boundaries, while fine grain structures improved the resistance to solidification cracking. Al-Cu-Mg alloys were often considered ''unweldable'' due to their low crack susceptibility (Ref 97). Gu et al. (Ref 47) reported that the cracking susceptibility of WAAMed Al-Cu-Mg alloys could be minimized by adjusting the Cu/Mg content ratio and they reported that the Al-(4.2–6.3)Cu-(0.8-1.5)Mg alloys had low sensitivity to cracking. Chi et al. (Ref 98) used the special Al-Cu-Mg wire nano-treated with TiC nanoparticles to produce Al-Cu-Mg alloys by GTAW-WAAM process. The crack-free Al-4.5Cu-1.4 Mg alloy wall components were successfully manufactured. The nanoparticle-modified secondary phase improved the liquid backfilling during the semisolid stage of solidification, thus mitigating the formation of solidification cracks (Ref 99). Qi et al. (Ref 100) reported that the double-wire GTAW-WAAM process was a feasible method to produce Al-Cu-Mg alloys with the low cracking susceptibility. The WAAMed Al-4.4Cu-1.5 Mg alloys showed excellent mechanical properties after heat treatment. Furthermore, the substitution of Mn for Mg to form Al-Cu-Mn series alloys not only can improve the cracking resistance, but also reduces the brittle temperature interval because the S-Al_2CuMg eutectic phases with more low melting point will be not formed. This is the main reason why the Al-Cu-Mn series alloys have good weldability.

In summary, to control crack defects, the following measures can be adopted: (1) optimize the compositions of the wires; (2) promote the formation of fine grain structures; (3) implement multi-wire WAAM processes; and (4) apply modifications of TiC or other nanoparticles.

4.4 Residual Stress and Deformation

Residual stress and deformation are inherent to the WAAM processes, relating to the physical nature of materials. Residual stress refers to the internal stress that still exists in the formed parts after machining, and it is impossible to avoid its occurrence completely. High residual stress can lead to the deformation and warpage of the formed parts, loss of geometric tolerance, reduction in fatigue performance, and even cracking (Ref 101, 102). Therefore, it is particularly important to control and minimize the residual stress and deformation.

Tawfik et al. reported that the formation of residual stress and deformation was related to the multiple thermal expansion and shrinkage processes under the influence of the thermal cycles, leading to the plastic deformation of materials if the remained stresses was higher than the yield strength (YS) but lower than the ultimate tensile strength (UTS), and fracture if it was greater than the UTS (Ref 103, 104). Similarly, Wang et al. (Ref 105) reported that the multi-times of melting and rapid solidification during WAAM are key reasons for the deformation of deposited parts. Debroy et al. (Ref 106) identified three key factors: (1) spatial temperature gradient generated by the local heating and cooling of the mobile heat source; (2) thermal expansion and shrinkage caused by multi heating and cooling; and (3) plasticity and flow stresses. Recent studies have shown that the surface treatment processes can effectively improve the distribution of residual stress and reduce the stress. Sun et al. (Ref 107) reported that the residual stresses of laser shock peening (LSP)-treated 2319 alloys fabricated by WAAM were modified from the tensile to compressive state with a maximum value around 100 MPa. Wang et al. (Ref 108) reported that applying ultrasonic impact treatment (UIT) process to treat the WAAMed 2219 alloys can both refine microstructure and reduce residual stress. After UIT with 1 and 2.5 A working current, the average compressive residual stress on the deposition surface decreased by 78.4 and 79.2%, respectively. Honnige et al. (Ref 109) reported the residual stresses of WAAMed 2319 alloy wall components could be improved significantly by introducing the interlayer rolling load, with plastic deformation reducing tensile residual stress and increasing compressive residual stress. In addition, the residual stress of WAAMed deposition might be related to the thickness of the

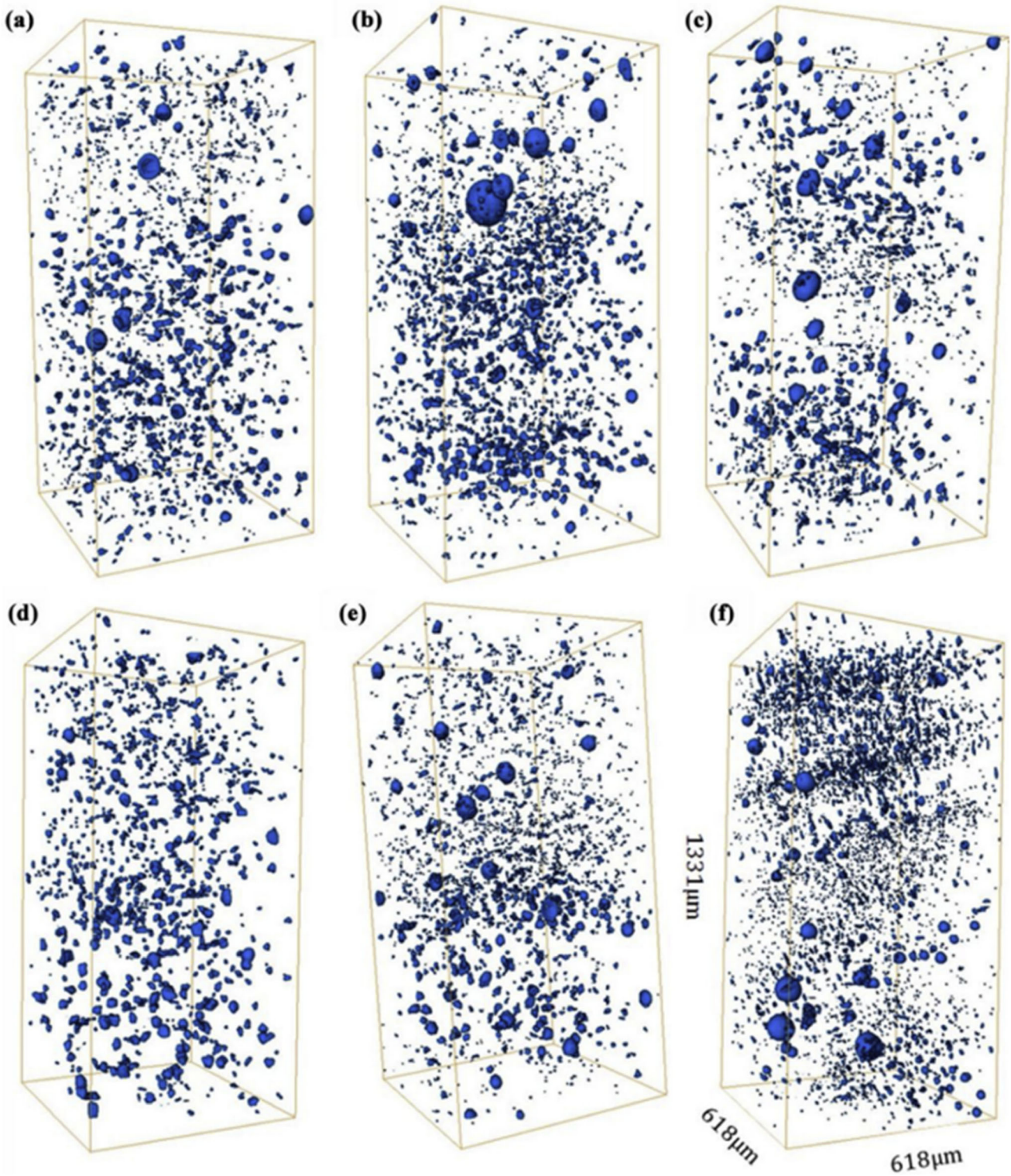

Fig. 10 3D views of micropores in the WAAM 2319 alloy with the state of as-deposited at locations of [94] (a) top, (b) middle, and (c) bottom; heat-treated at (d) top, (e) middle, and (f) bottom. Reprinted from *Additive Manufacturing,* Vol 30, J. Gu, M. Gao, S. Yang, J. Bai, J. Ding, X. Fang, Pore formation and evolution in wire + arc additively manufactured 2319 Al alloy, Article 100,900, Copyright 2019, with permission from Elsevier

substrate. As reported as Derekar et al. (Ref 110), greater residual stresses were found in specimens produced by using a 20-mm substrate than those of a 6-mm substrate.

Therefore, the non-uniform thermal cycles are the main factors, leading to the development of residual stress and deformation. However, it is still challenging to control residual

stress and deformation solely optimizing thermal recycles. Fortunately, several surface treatment processes have been proven to effectively reduce the strength losses caused by residual stress and deformation.

5. Mechanical Properties and its Strategies for Improvement of the WAAMed Al-Cu Alloys

The mechanical properties of the WAAMed Al-Cu alloys are highly dependent on the microstructure and defects. Table 2 summarizes the mechanical properties of the typical WAAMed Al-Cu alloys in the horizontal direction. It can be observed that the UTS, YS, and elongation of the traditional WAAMed 2319 alloys are 260 MPa, 125 MPa, and 16%, respectively. After the T6 heat treatment, the UTS, YS, and elongation of the WAAMed 2319 alloys are 460 MPa, 330 MPa, and 14%, respectively. The 205A alloy, which is the modified Al-Cu alloy by adding Cd, shows the excellent mechanical properties (UTS: 510 MPa, YS: 460 MPa, and elongation: 11.8%) after the T6 heat treatment due to the grain refinement and the precipitation strengthening increased by Cd (Ref 84). Jin et al. (Ref 90) reported that the diffusely distributed TiC particles weakened the segregation at the grain boundaries and possessed a coherent interface with θ-Al_2Cu phases, which improved synergistically the strength and elongation of the as-deposited 2219 alloys. The UTS, YS, and elongation of the as-deposited alloys were 384 MPa, 270 MPa, and 18.3%, respectively. Fang et al. (Ref 111) reported that the interlayer hammering process greatly enhanced the strength of the WAAMed 2319 alloy due to the grain refinement and the increase in dislocation density. Under the influence of 50.8% deformation of the interlayer hammering, the UTS and YS of the as-deposited alloy increased by 17.2 and 60.7%, respectively, to reach 334 and 241 MPa. However, the elongation decreased from 18 to 12.5%. Gu et al. (Ref 67) found that although the interlayer rolling process reduced the elongation of the as-deposited 2319 alloys from 18.5 to 8.5%, the elongation of the T6 heat-treated specimens was significantly increased to 17.5% because of the inhibition of pore defects, as shown in Fig. 11. It is noteworthy that the strength of the rolled alloys is close to that of the treated specimens in the T6 heat treatment conditions due to the loss of dislocation density during heat treatment process. Wei et al. (Ref 53) employed the friction stir process hybrid additive manufacturing process to deposit 2319 alloy components, leading to the significantly improvements in the strength and elongation of the as-deposited specimens due to the remarkable grain refinement, broken-up of the second phases, and elimination of pores induced by friction stir process deformation, especially in terms of elongation. The elongation of the treated 2319 alloys is 23.7% in the horizontal direction, far exceeding that of 2319 alloys fabricated by other WAAM processes. Qi et al. (Ref 100) reported that the UTS, YS, and elongation of the Al-4.4Cu-1.5 Mg alloys fabricated by double-wire GTAW-WAAM process were 284 MPa, 177 MPa, and 6%, respectively. After the T6 heat treatment, the UTS, YS, and elongation of the heat-treated Al-4.4Cu-1.5 Mg alloys were 470 MPa, 374 MPa, and 8.2%, respectively. Cong et al. (Ref 35) produced the Al-4.57Cu-1.32 Mg alloys by double-wire GTAW-WAAM process with the UFPVP as heat source. The UTS, YS, and elongation of the T6 heat-treated specimens were 471 MPa, 302 MPa, and 14%, respectively, which were superior to Al-4.4Cu-1.5 Mg alloys fabricated by traditional double-wire GTAW-WAAM process. Gu et al. (Ref 56) developed a new Al-4.3Cu-1.5 Mg alloy wire and deposited the Al-4.3Cu-1.5 Mg alloy thin-wall components by single-wire CMT-WAAM process. The UTS, YS, and elongation of the T6 heat-treated Al-4.3Cu-1.5 Mg alloys were 485 MPa, 399 MPa, and 9%, respectively. It can be found that the advantages of WAAMed Al-Cu-Mg series alloys are their strengths, while the elongations are lower, compared with Al-Cu-Mn series alloys. Chi et al. (Ref 98) developed a new Al-4.7Cu-1.53 Mg-1.26Ti alloy wire nano-treated by TiC parti-

Table 2 Mechanical properties of WAAMed Al-Cu alloys by various processes in the horizontal direction

Materials	Processes	As-deposited			Post-processing		
		UTS, MPa	YS, MPa	Elongation, %	UTS, MPa	YS, MPa	Elongation, %
2219-Al (Ref 67)	45kN interlayer rolling	253	127	18.5	320	250	8.5
	T6 heat treatment				465	330	14
	45kN interlayer rolling + T6 heat treatment				460	320	17.5
2319-Al (Ref 111)	50.8% deformation of interlayer hammering	285	150	18	334	241	12.5
2219-Al (Ref 107)	Laser shock peening	250	105	12.5	245	175	6
2319-Al (Ref 53)	Interlayer + FSP	250	98	17.7	279	108	23.7
2319-Al (Ref 95)	In situ rolled				279.6	152.7	15.3
	In situ rolled + T6 heat treatment				454.4	356.6	14.4
2319-Al(1.5Ti) (Ref 90)	TiC particles treated deposits				384	270	18.3
205A-Al (Ref 84)	T6 heat treatment	249.7	103.2	11.2	510.2	459.5	11.8
Al-4.4Cu-1.5 Mg (Ref 100)	D-WAAM + T6 heat treatment	284	177	6	470	374	8.2
Al-4.3Cu-1.5 Mg (Ref 56)	T6 heat treatment	293	185	12	485	399	9
Al-4.7Cu-1.5 Mg-1.26Ti (Ref 98)	TiC particle-treated wire + T6 heat treatment	328	166	8	428	324	7.4
Al-4.57Cu-1.32 Mg (Ref 35)	D-UFPVP WAAM + T6 heat treatment	284	177	6	471	302	14

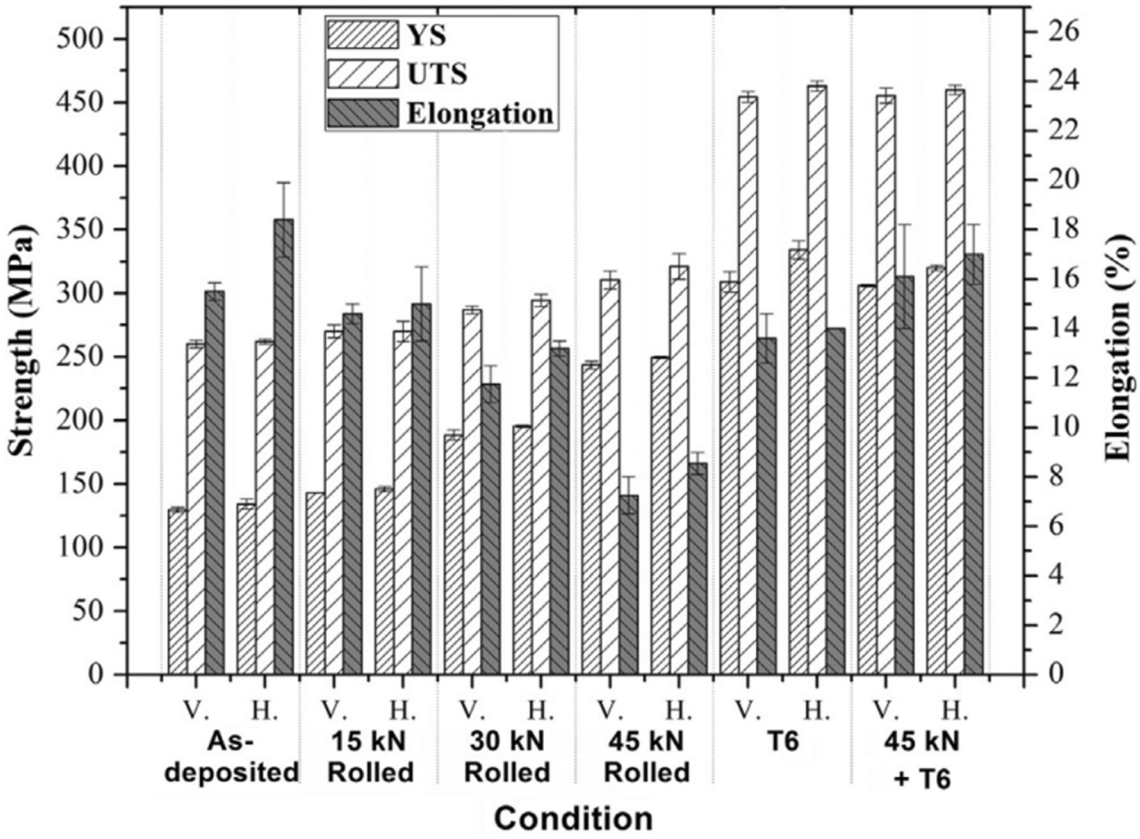

Fig. 11 Tensile properties of the as-deposited, interlayer-rolled, and heat-treated WAAM 2219 alloys (where V represents the vertical direction and H represents the horizontal direction) [67]. Reprinted from *Materials Science and Engineering: A,* Vol 651, J. Gu, J. Ding, S.W. Williams, H. Gu, J. Bai, Y. Zhai, P. Ma, The strengthening effect of inter-layer cold working and post-deposition heat treatment on the additively manufactured Al–6.3Cu alloy, Pages 18–26, Copyright 2016, with permission from Elsevier

cles. Although the WAAMed Al-Cu-Mg alloy components were crack-free, the strength (UTS: 428 Mpa and YS: 324 Mpa) was significantly lower than other WAAMed Al-Cu-Mg alloys.

The mechanical properties of the WAAMed Al-Cu alloys in the horizontal and vertical directions are shown in Fig. 12. It can be found that the WAAMed Al-Cu alloys generally show the anisotropic characteristics (the distance between two points reflects the degree of anisotropic). Furthermore, the lower properties of the WAAMed Al-Cu alloys in the vertical direction are observed. Gu et al. (Ref 56) reported that the weak areas of the interlayer regions were caused by the complex microstructure and more serious pore defects, as shown in Fig. 13. Therefore, the strength of the as-deposited alloy in the vertical direction is significantly lower than that of the horizontal direction. Furthermore, they reported that the lower elongation of Al-4.3Cu-1.5 Mg alloy fabricated by single-wire WAAM process in the vertical direction was also attributed to the presence of the interlayer microcracks (Ref 56). Comparatively, the Al-4.7Cu-1.5 Mg-1.26Ti alloys fabricated by single-wire WAAM process showed lower strengths than the Al-4.3Cu-1.5 Mg alloys, but the elongations of the Al-4.7Cu-1.5 Mg-1.26Ti alloys were 7.4% in both directions due to the eliminate of cracks (Ref 98).

In summary, the mechanical properties of the WAAMed Al-Cu alloys can be enhanced by (1) improving the arc source; (2) developing new Al-Cu alloy wires; (3) employing the interlayer cold working processes; and (4) applying post-processing processes. Furthermore, it is essential to inhibit the anisotropic properties. Additionally, the studies on reducing the cracking sensitivity of the WAAMed Al-Cu-Mg alloys are highly significant and should be further explored.

6. Post-Processing Process

Post-processing processes are adopted to improve the quality and properties of the WAAMed Al-Cu alloy components and reduce defects such as inhomogeneous microstructure, pores, and residual stress and deformation. To achieve this, several post-processing processes have been developed and their latest developments are discussed in this section.

6.1 Heat Treatment

Heat treatment process is widely used in the multiple engineering alloys to improve the microstructure and mechanical properties (Ref 23, 67, 112). Two-series Al-Cu alloys belong to the heat-treatable strengthening aluminum alloy. Depending on the alloy systems, service temperature, and heat treatment conditions, the appropriate heat treatment process should be selected. Otherwise, problems such as over-burning, grain coarsening, and improper sizes and morphology of precipitated phases may arise, affecting the mechanical properties of WAAMed Al-Cu alloys adversely.

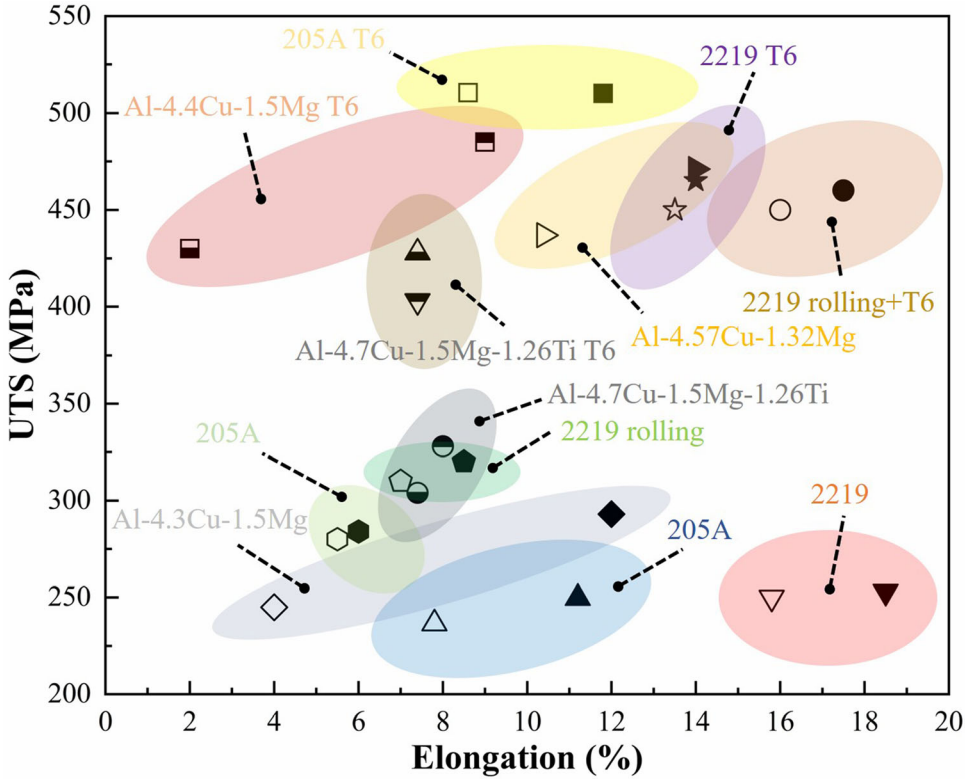

Fig. 12 Mechanical properties of WAAMed Al-Cu alloys in the horizontal and vertical directions (the solid pattern and the upper half solid pattern are in the horizontal direction, while the opposite is in the vertical direction) [56, 67, 84, 98, 100]

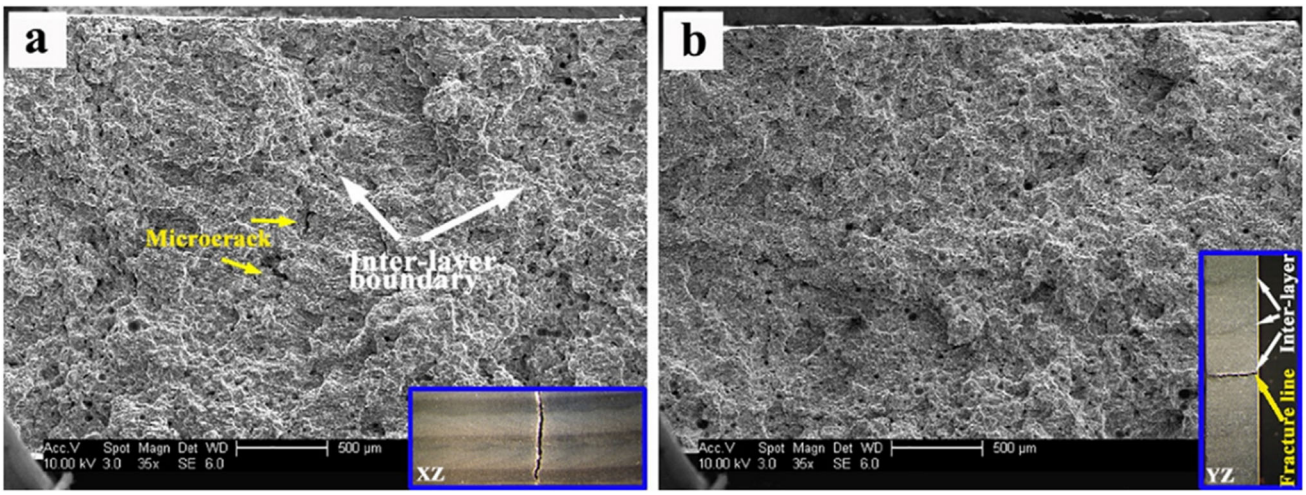

Fig. 13 Side view and fractographic morphology of fractured tensile samples for as-deposited alloy with loading direction in [56] (a) horizontal and (b) vertical. Reprinted from *Materials and Design,* Vol 186, J. Gu, M. Gao, S. Yang, J. Bai, Y. Zhai, J. Ding, Microstructure, defects, and mechanical properties of wire + arc additively manufactured Al Cu4.3-Mg1.5 alloy, Article 108,357, Copyright 2020, with permission from Elsevier

Table 3 summarizes the heat treatment processes of the WAAMed Al-Cu alloys and their elongation changes before and after heat treatment. It can be observed that the T4 heat treatment (solution treatment + natural aging treatment) and T6 heat treatment (solution treatment + artificial aging treatment) are commonly used to enhance the mechanical properties of the WAAMed Al-Cu alloys. Moreover, the elongations of the WAAMed Al-Cu alloys generally reduced after T6 heat treatment.

Qi et al. (Ref 113) investigated the effects of different solution temperature on the performances of the T4 heat-treated Al-4.4Cu-1.5 Mg alloys fabricated by double-wire GTAW-WAAM process. The micro-hardness of the T4 heat-treated alloys was 135 HV, 138 HV, and 143 HV at 485, 498, and 503 °C, respectively, and the highest UTS and elongation of the T4 heat-treated alloys were 497 MPa and 16%, respectively, at 503 °C. After the T4 heat treatment, the main second phases were transformed from α-Al, θ-Al_2Cu, and S-Al_2CuMg to α-Al

Table 3 Heat treatment processes of the WAAMed Al-Cu alloys (where V represents the vertical direction and H represents the horizontal direction)

Materials	Manufacturing processes	Heat treatment system	As-deposited, H/V, %	Heat-treated, H/V, %
2219-Al (Ref 121)	GTAW-WAAM	530 °C/20 h + 175 °C/17 h	10.7/10.6	10.2/7.4
2319-Al (Ref 67)	CMT-WAAM	535 °C/1.5 h + 175 °C/3 h	18.5/15.8	14/13.5
	CMT-WAAM + interlayer rolling	535 °C/1.5 h + 175 °C/3 h		17.5/16
2319-Al (Ref 95)	GMAW-WAAM + interlayer in situ rolling	535 °C/1.5 h + 175 °C/3 h	15.3	16
205A (Ref 84)	CMT-WAAM	538 °C/12 h + 175 °C/4 h	11.2/7.8	11.8/8.6
Al-4.3Cu-1.5 Mg (Ref 56)	CMT-WAAM	498 °C/1.5 h + 190 °C/6 h	12/4	9/2
Al-4.4Cu-1.5 Mg (Ref 100)	D-WAAM	498 °C/1.5 h + 190 °C/6 h	6/5.5	8.2/2
Al-4.4Cu-1.5 Mg (Ref 113)	D-WAAM	485 °C/1.5 h + natural aging	6	8.6
		498 °C/1.5 h + natural aging		12.7
		503 °C/1.5 h + natural aging		16
Al-4.7Cu-1.53 Mg-1.26Ti (Ref 98)	GTAW-WAAM	493 °C/1 h + 190 °C/12 h	11.2	11.8

and θ-Al_2Cu. Gu et al. (Ref 67) reported that the different sized incoherent stable θ phases were observed in the as-deposited 2219 alloys, as shown in Fig. 14(a). After the 535 °C/1.5 h + 175 °C/3 h heat treatment, the fine needle-like precipitates θ' were found to be densely and homogeneously distributed in the matrix, as shown in Fig. 14(b). The UTS of the WAAMed Al-Cu alloys was increased from 253 to 465 MPa in the horizontal direction, while the elongation was reduced from 18.5 to 14%. Zhou et al. (Ref 84) deposited 205A alloys using a CMT heat source, and the specimens were solutionized at 538 °C for 12 h and then artificially aged at 175 °C for 4 h. The good coherent relationships between precipitates (θ'' and θ') and α-Al can be found, as shown in Fig. 15. Due to the addition of Cd elements promoting the precipitations of dense and homogeneous θ' phase in the WAAMed Al-Cu alloys, the UTS of the WAAMed 205A alloys was 510.2 MPa in the horizontal direction. Gu et al. (Ref 56) produced the Al-4.3Cu-1.5 Mg alloys using CMT-WAAM process, and the deposits were T6 heat treated (498 °C/1.5 h + 190 °C/6 h). They reported that the presence of the fine rod-shaped orthorhombic T-$Al_{20}Cu_2Mn_3$ phases with the typical length of 80-400 nm and aspect ratio ranging from 2 to 6 caused dislocation tangling under plastic deformation, which resulted in the higher strength of the as-deposited WAAMed Al-4.3Cu-1.5 Mg alloy than the WAAMed Al-6.3Cu alloy. After the T6 heat treatment, the precipitations of high-density needle-shaped S' phases and few T phases significantly improved the strengths of the WAAMed Al-4.3Cu-1.5 Mg alloy by resisting dislocation slip and trapping dislocations.

In summary, the mechanical properties of the WAAMed Al-Cu alloys can be significantly improved by means of heat treatment processes, due to the elimination of inhomogeneous microstructures, and the precipitation of homogeneous dispersion strengthening phases. However, the heat treatment process causes a general decrease in the elongation of the heat-treated alloy, as the porosity defects present in the as-deposited alloy are worsened. Fortunately, recent studies have indicated that the several cold working processes can compensate for the loss of elongation caused by the deterioration of pore defects during heat treatment processes (Ref 95, 114). Additionally, according to the results of Qi et al. (Ref 113), the T4 heat treatment process may be considered for improving the elongation of the WAAMed Al-Cu alloys. Therefore, the selection of suitable heat treatment processes and the inhibition of pore defect deterioration are key to achieving superior mechanical properties of the heat-treated WAAM Al-Cu alloys.

6.2 Interlayer Cold Working

The work hardening is one of the major strengthening mechanisms pertinent to the materials. Recent studies have identified that the work-hardened Al-Cu alloys fabricated by WAAM show excellent microstructure and mechanical properties by interlayer cold working processes.

Gu et al. (Ref 67) investigated the influence of different interlayer rolling loads (15, 30, and 45 kN) on the microstructure and mechanical properties of the WAAMed 2319 alloys. The interlayer rolling loads reduced the mean height per layer of the deposits from 2.35 to 1.31 mm and increased the mean wall width from 6.8 to 11.5 mm, resulting in a deformation of 13.2%, 30%, and 44.2% at 15 kN, 30 kN, and 45 kN loads, respectively. They reported that the grain structures were gradually refined as the increase in interlayer rolling loads, elongating along the short-transverse direction. Additionally, the size and density of the dimples were increased gradually with the increasing interlayer rolling load, which indicated an increase in strength (Ref 115). Honnige et al. (Ref 109) introduced two different rolling techniques (interlayer rolling process and post-deposition rolling process) to treat the WAAMed 2319 alloy thin-wall components, and the schematics of these rolling techniques are shown in Fig. 16. They reported that the height of the deposits was significantly reduced by interlayer rolling process, while there was little effect in height for the post-deposition rolled specimens. The surface waviness was increased by introducing the interlayer rolling process, while it was smoothened by applying post-deposition rolling processes. These rolling processes increased the hardness of the deposits due to the work hardening. Additionally, they found that the post-deposition side rolling was more effective for controlling residual stress and deformation. Fang et al. (Ref 111) employed the interlayer hammering process to strengthen the WAAMed 2319 alloy components and investigated the influence of different deformation degree (0, 21.8, and 50.8%) on the microstructure and

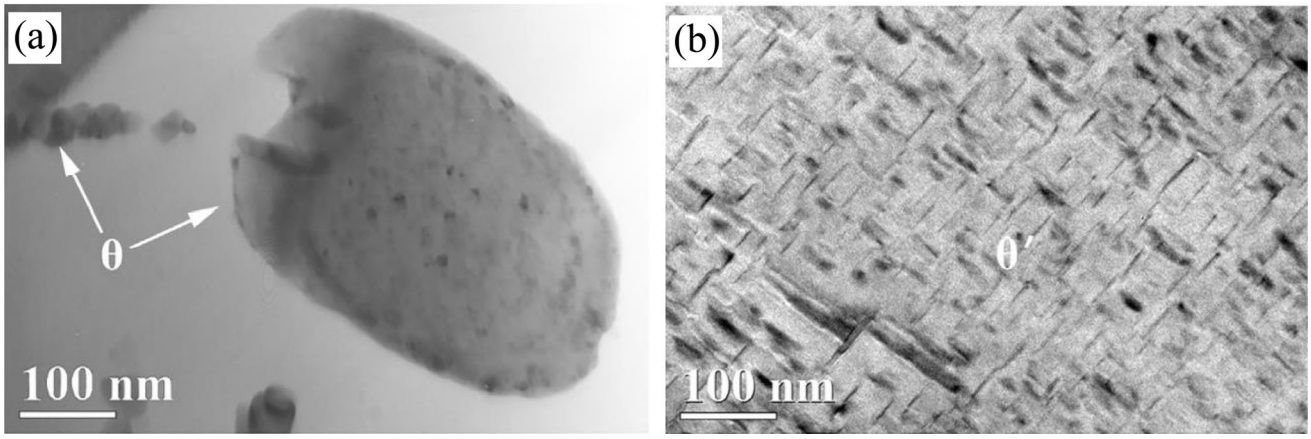

Fig. 14 Transmission electron microscopy images of the WAAMed 2219 alloys [67]: (a) as-deposited (taken from the third layer beneath the top surface of the wall) and (b) after-deposition T6 treated. Reprinted from *Materials Science and Engineering: A,* Vol 651, J. Gu, J. Ding, S.W. Williams, H. Gu, J. Bai, Y. Zhai, P. Ma, The strengthening effect of inter-layer cold working and post-deposition heat treatment on the additively manufactured Al–6.3Cu alloy, Pages 18–26, Copyright 2016, with permission from Elsevier

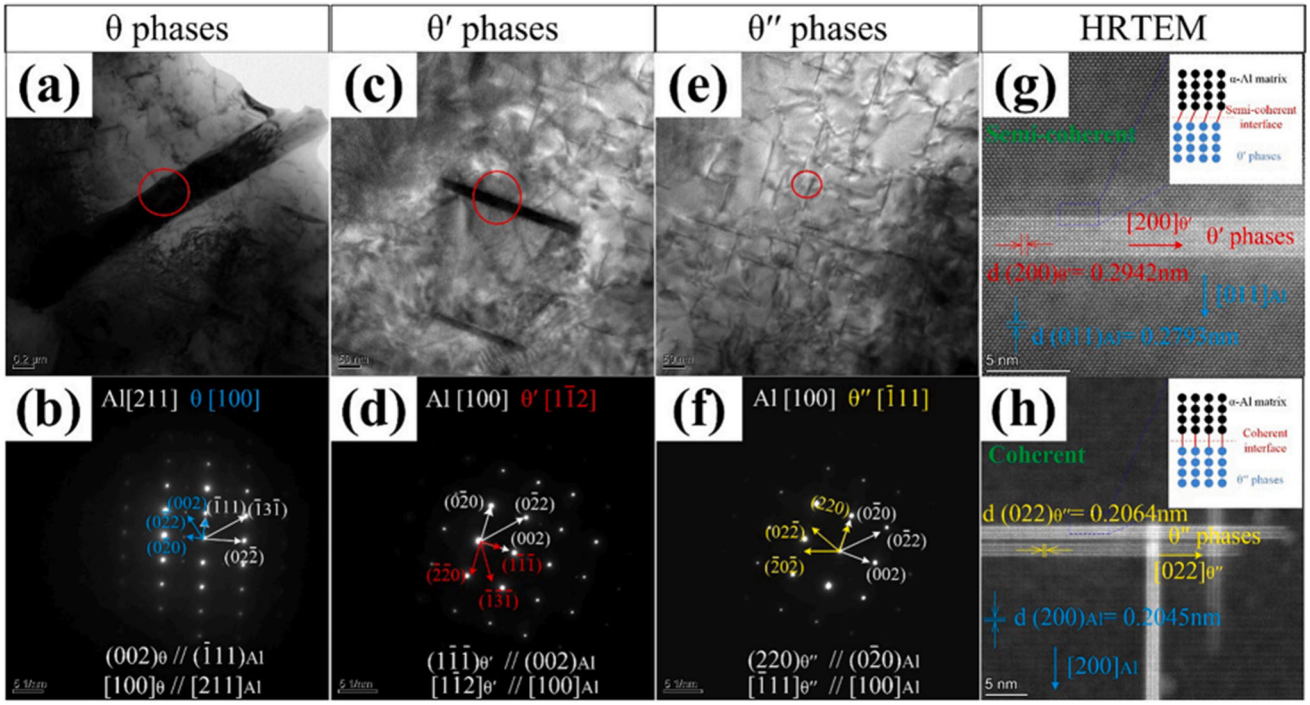

Fig. 15 The TEM images [84]: (a) θ phase; (c) θ' phase; (e) θ'' phase; the SAED image: (b) θ phases and α-Al matrix; (d) θ' phases and α-Al matrix; (f) θ'' phases and α-Al matrix; the high-resolution transmission electron microscopy (HRTEM) images between α-Al matrix and Al-Cu phases: (g) coherent and (h) semi-coherent situations. Reprinted from *Materials Characterization,* Vol 189, S. Zhou, K. Wu, G. Yang, B. Wu, L. Qin, H. Wu, C. Yang, Microstructure and mechanical properties of wire arc additively manufactured 205A high strength aluminum alloy: The comparison of as-deposited and T6 heat-treated samples, Article 111,990, Copyright 2022, with permission from Elsevier

mechanical properties. The mean single-layer height was reduced from 2.69 to 1.22 mm, resulting in a deformation of 0, 21.8, and 50.8%, respectively. GE x-ray computed tomography was applied to observe the change in porosity before and after interlayer hammering process. Figure 17 shows the results of microstructure and porosity. It can be clearly seen that the microstructure was significantly refined and most of pores were closed by applying interlayer hammering process. However, according to their reports, although the interlayer hammering process effectively closed the porosity, the elongation decreased from 18% (0% deformation) to 12.5% (50.8% deformation). Wang et al. (Ref 95) employed the in situ rolled WAAM process to produce 2319 alloy components. They reported that the majority of the solidification shrinkage cavities were eliminated during WAAM by introducing in situ rolling process. However, after the T6 heat treatment, the fine hydrogen pores with high density were formed due to the hydrogen micropore precipitation.

The primary goal of the interlayer cold working processes is to enhance the overall performance of the WAAMed Al-Cu

alloys by refining the microstructure, minimizing pore defects, reducing residual stress, and introducing dislocation to increase strengths. It also helps to prevent the rapid decrease in the elongations of the WAAMed Al-Cu alloys after the T6 heat treatment by reducing pore density. In recent years, these interlayer cold working processes have been recognized as the effective way to improve the forming quality and performance of the WAAMed Al-Cu alloys. However, it is important to note that these currently available processes may only be suitable for the simple additive manufacturing parts, such as wall components. Consequently, further development needs to take into account the applicability to complex structures as well as the development of additional processes.

6.3 Surface Treatment

In recent years, several surface treatment processes have been employed to improve the performance of the WAAMed Al-Cu alloys after deposition.

Laser shock peening (LSP) is an effective surface treatment process which utilizes a high-power-density pulse laser and ultra-short duration onto the surface of components to induce large depth and high value compressive residual stress to relieve the tensile stress (Ref 116, 117). Sun et al. (Ref 107) used a Q-switched Nd:YAG high-power pulse laser (wavelength: 1064 nm and pulse duration: 15 ns) to treat the 2319 alloy thin-wall components fabricated by GTAW-WAAM process. It can be found that the LSP could effectively improve the micro-hardness, as shown in Fig. 18(a). However, the hardness improvement decreased to the level of untreated samples gradually with increasing the penetration depth. Moreover, residual stress in both the topmost and middle sections was modified from tensile stress to compressive residual stress after LSP. The maximum value of compressive residual stress was around 100 MPa and an affected depth was more than 0.75 mm, but the effect of LSP on residual stress also decreased with increasing the penetration depth, as shown in Fig. 18(b). Ultrasonic impact treatment (UIT) is a surface strengthening process that adopts the impact energy to produce large plastic deformation onto the deposit surface, refining grain structures and generating the compressive stress to relieve tensile stress (Ref 118). Wang et al. (Ref 108) deposited 2319 alloy thin-wall components fabricated by CMT-WAAM process and treated them with the UIT (working currents were 1 A and 2.5 A, respectively). It can be observed that the grain structures were refined significantly after UIT process, as shown in Fig. 19. When the working current was low (1 A), some columnar grains were found in the microstructure due to the limited plastic deformation zone. When the working current increased to 2.5 A, fine equiaxed grains evenly distributed were observed, indicating a significant improvement in the grain refinement. In addition, pore defects and surface residual stress were significantly improved after UIT process.

Both LSP and UIT processes use high-energy medium to impact samples and release the internal stress by exerting compressive stress onto the surface of components. Their advantages are reflected in: (1) refining microstructure; (2) eliminating pore defects; (3) improving hardness; and (4) reducing residual stress. However, their strengthening effects decrease with the increasing penetration depth, making them have negligible effects on medium or large components fabricated by WAAM.

7. Outlook

Currently, there are numerous studies concerning Al-Cu alloys fabricated by WAAM, which strive to improve the forming quality, microstructure, and mechanical properties through optimizing WAAM processes, designing novel Al-Cu wires and employing post-process processes. However, it is necessary to summary some concepts to direct the future research into the aspects. This section provides some examples, some of which are generic in nature that they can be applied to WAAM processes regardless of the materials being produced.

Wire quality and composition have a significant effect on the performance of WAAMed alloys (Ref 92). Therefore, it is important to design and develop dedicated WAAM wires by adding other micro-alloying elements or TiC particle. Micro-alloying elements such as Ti, Zr, Sc, La, Ce, Cd, and Sn can be added to Al-Cu alloy wires according to previous studies. Some of them contribute to the microstructure refinement, and some are conducive to improve the performance of heat-treated Al-Cu alloys. Additionally, TiC nanoparticles have been proven to reduce the crack sensitivity of Al-Cu-Mg alloys in the field of selective laser melting (SLM) processes (Ref 119, 120). Recent studies show that it is also suitable for the WAAMed Al-Cu alloys, and crack-free Al-Cu-Mg alloy components have been manufactured by adding TiC nanoparticles into Al-Cu-Mg alloy wire (Ref 98). This technology liberates the embarrassing situation of Al-Cu-Mg alloys in the field of WAAM due to their high sensitivity to hot cracks. However, although limited by the difficulty of wire production, related progress may be slow, it is an important way that will contribute to the development of WAAM alloys in future, not just for aluminum alloys.

Studies on addressing the defects present in the WAAMed Al-Cu alloy deposits have largely focused on the interlayer cold working and surface treatment processes. Surface treatment processes offer advantages in terms of improving microstructure and relieving residual stress, yet their efficacy is limited by penetration depth and additional time and cost involved. In contrast, the interlayer cold working processes such as interlayer rolling and interlayer hammering play an essential role in enabling near-net-shaped WAAM processes, as they can enhance the quality of WAAMed components while preserving their forming efficiency. Thus, further exploration into the synergistic effects between WAAM and cold working processes will be critical for the WAAM of all materials.

The heat treatment process is a key part of improving the performance of WAAMed Al-Cu alloys. The current studies focus on the T4 and T6 heat treatment processes. To further improve the microstructure and mechanical properties, other heat treatment processes, such as T8 heat treatment process (solution treatment + cold working + artificial aging), can be considered. This heat treatment process theoretically avoids the deterioration of alloy performance caused by porosity defects during high temperature heat treatment process. Moreover, if component needs to go through interlayer cold working process during WAAM, the selection of heat treatment process should be adapted in order to prevent a decrease in performance due to abnormal recrystallization during heat treatment.

As a future development, the main application area for WAAMed Al-Cu alloys is the aerospace industry. To meet the demands of this industry, the WAAM process should be developed to achieve the forming of complex shapes. In

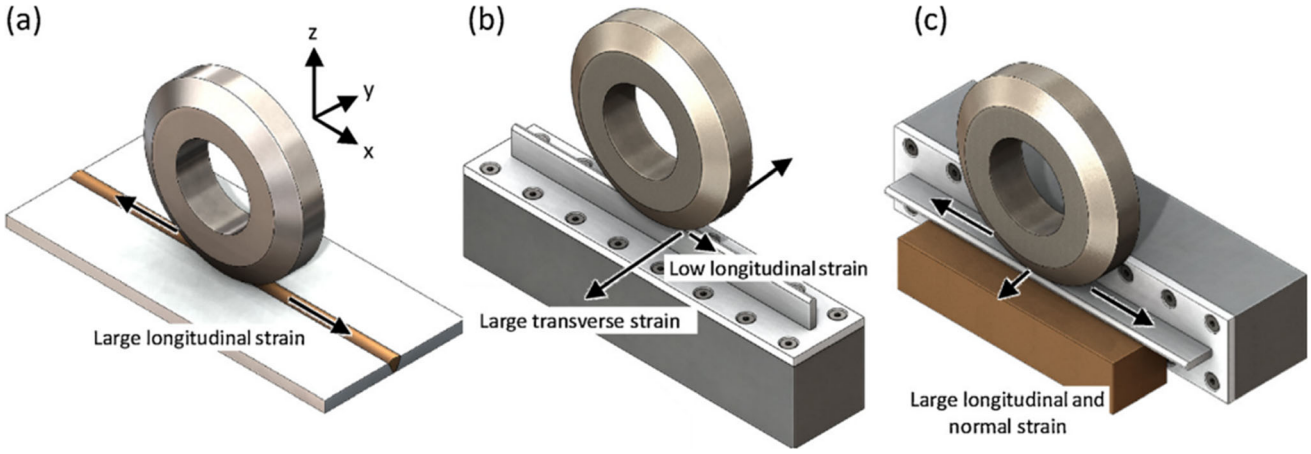

Fig. 16 Main directions of strain induced by cold rolling [109]: (a) vertical rolling of butt welds; (b) vertical rolling of WAAM wall; and (c) side rolling of WAAM wall. Reprinted from *Additive Manufacturing,* Vol 22, J.R. Hönnige, P.A. Colegrove, S. Ganguly, E. Eimer, S. Kabra, S. Williams, Control of residual stress and distortion in aluminium wire + arc additive manufacture with rolling, Pages 775–783, Copyright 2018, with permission from Elsevier

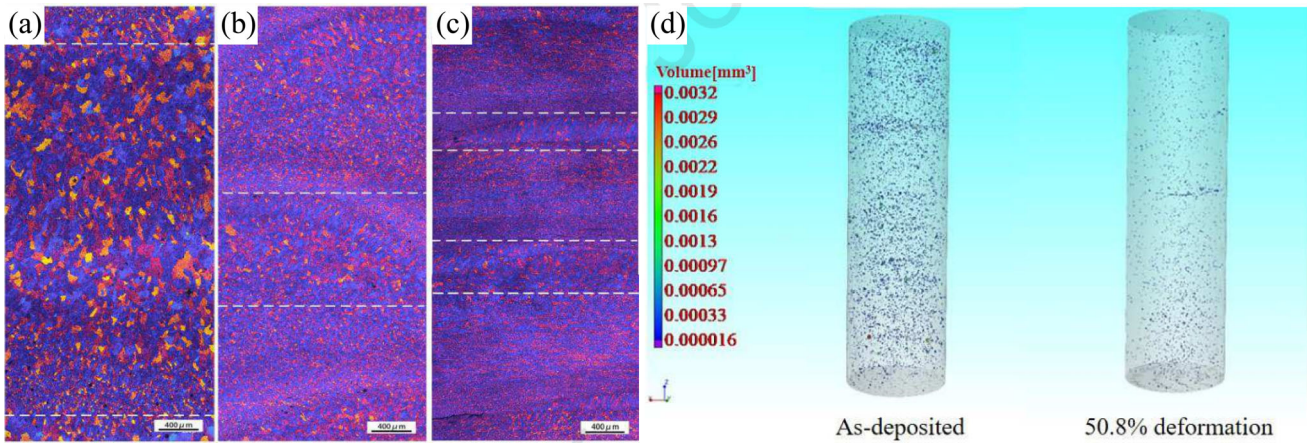

Fig. 17 Micrographs of samples with different deformations of (a) 0%, (b) 21.8%, (c) 50.8%, and (d) pores distribution in as-deposited and deformed sample [111]. Reprinted from *Materials Science and Engineering: A,* Vol 800, X. Fang, L. Zhang, G. Chen, K. Huang, F. Xue, L. Wang, J. Zhao, B. Lu, Microstructure evolution of wire-arc additively manufactured 2319 aluminum alloy with interlayer hammering, Article 140,168, Copyright 2021, with permission from Elsevier

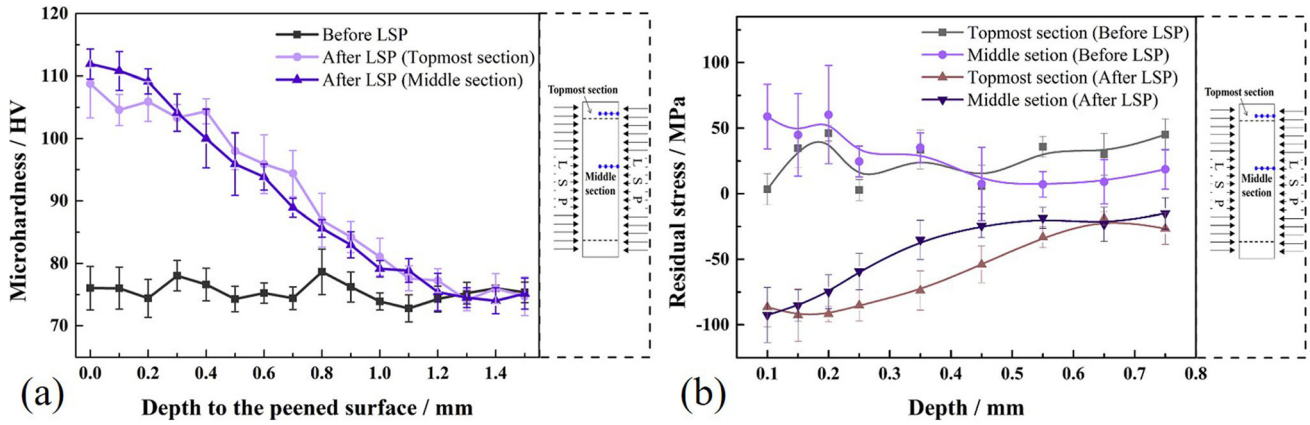

Fig. 18 (a) Micro-hardness distributions in the depth direction before and after LSP and (b) in-depth residual stress in the topmost section and middle section before and after LSP [107]. Reprinted from *Journal of Alloys and Compounds,* Vol 747, R. Sun, L. Li, Y. Zhu, W. Guo, P. Peng, B. Cong, J. Sun, Z. Che, B. Li, C. Guo, L. Liu, Microstructure, residual stress and tensile properties control of wire-arc additive manufactured 2319 aluminum alloy with laser shock peening, Pages 255–265, Copyright 2018, with permission from Elsevier

addition, the hybrid WAAM processes should be adapted to the production of complex shape parts and further integrated into industrial production through digital automation and robot-assisted equipment, in order to gain control over shape and performance. Of course, further studies need to be further developed in areas such as forming path planning and residual stress relief to expand its application areas.

8. Conclusion

This paper reviews the latest technological developments of WAAMed high-strength Al-Cu alloys, focusing on the solidification microstructure, common defects, mechanical properties, and post-processing processes. From this review, the following conclusions can be drawn:

(1) The typical solidification microstructure of WAAMed Al-Cu alloys typically exhibits an alternating distribution of coarse columnar grains and fine equiaxed grains, which is attributed to the inhomogeneous thermal cycles and alloy composition. The microstructure can be effectively improved by optimizing the manufacturing process, adjusting the welding parameters, and optimizing the alloy composition. In particular, alloying elements have a marked effect for improving the microstructure and mechanical properties of WAAMed Al-Cu alloys.

(2) Common defects in the WAAMed Al-Cu alloys include the inhomogeneous microstructure, pores, cracks and residual stress, and these issues combined lead to anisotropic properties. Despites significant efforts to improve them, heat-treated Al-Cu alloys still present a challenge in resolving the anisotropy properties.

(3) In order to overcome the loss of strength and elongation produced by pore defects, etc., the hybrid WAAM process has been increasingly investigated in recent years, such as interlayer rolling process. It has been proven that the hybrid WAAM process is effective in: (1) reducing pore defects; (2) refining microstructure; (3) improving forming quality and performance; and (4) releasing residual stress. However, the drawbacks of the hybrid

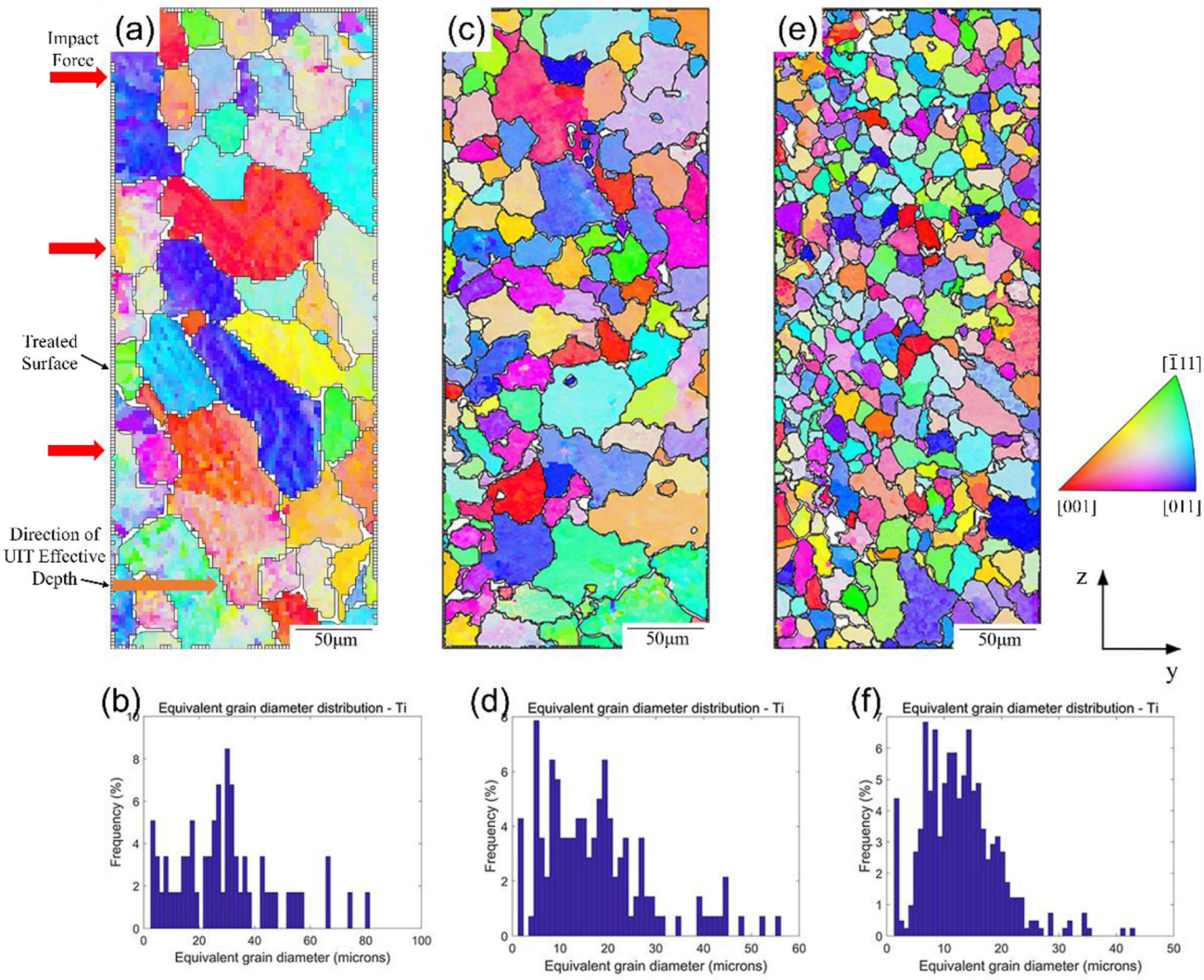

Fig. 19 Inverse pole figure and frequency histogram of specimens [108]: (a, b) AD state; (c, d) UIT-1 state and (e, f) UIT-2.5 state. Reproduced from *Journal of Materials Research and Technology,* Influence of ultrasonic impact treatment and working current on microstructure and mechanical properties of 2219 aluminium alloy wire arc additive manufacturing parts, by C.R. Wang et al. under the CC BY license

WAAM processes include their high equipment cost, more parameters involved in the process, and the potential to produce high complexity parts. Consequently, the cost-effective application of the hybrid WAAM process needs to be discussed and planned.

(4) With the advancement of new generation of wires and hybrid WAAM processes, the manufacture of Al-Cu alloy components by WAAM process is anticipated to be an effective technology in the aerospace industry due to its high material utilization, short production cycles, and reliable performance. Thus, further research should not only concentrate on improving the microstructure and properties, but also consider issues such as forming path planning and residual stress relief.

Acknowledgements

This research was funded by the Key Project of Research and Development in Yunnan Province, grant numbers 202103AN080001-002 and 202202AG050007-4, and the Key Project of Yunnan Fundamental Research, grant number 202101AS070017.

Conflict of interest

The authors declare no conflict of interest.

References

1. B. Li, L. Wang, B. Wang, D. Li, J.P. Oliveira, R. Cui, J. Yu, L. Luo, R. Chen, Y. Su, J. Guo and H. Fu, Electron Beam Freeform Fabrication of NiTi Shape Memory Alloys: Crystallography, Martensitic Transformation, and Functional Response, *Math. Sci. Eng. A-Struct.*, 2022, **843**, p 143135
2. F.F. Conde, J.A. Avila, J.P. Oliveira, N. Schell, M.F. Oliveira and J.D. Escobar, Effect of the As-Built Microstructure on the Martensite to Austenite Transformation in a 18Ni Maraging Steel After Laser-Based Powder Bed Fusion, *Addit. Manuf.*, 2021, **46**, p 102122
3. N.T. Aboulkhair, M. Simonelli, L. Parry, I. Ashcroft, C. Tuck and R. Hague, 3D Printing of Aluminium Alloys: Additive Manufacturing of Aluminium alloys using selective laser melting, *Prog. Mater. Sci.*, 2019, **106**, p 10057
4. F. Dababneh and H. Taheri, Investigation of the Influence of Process Interruption on Mechanical Properties of Metal Additive Manufacturing Parts, *CIRP J. Manuf. Sci. Tec.*, 2022, **38**, p 706–716
5. Y. Zhong, Z. Zheng, J. Li and C. Wang, Fabrication of 316L Nuclear Nozzles on the Main Pipeline with Large Curvature by CMT Wire Arc Additive Manufacturing and Self-Developed Slicing Algorithm, *Math. Sci. Eng. A-Struct.*, 2021, **820**, p 141539
6. K. Oyama, S. Diplas, M. M'Hamdi, A.E. Gunnæs and A.S. Azar, Heat Source Management in Wire-Arc Additive Manufacturing Process for Al-Mg and Al-Si Alloys, *Addit. Manuf.*, 2019, **26**, p 180–192
7. K.S. Derekar, A Review of Wire Arc Additive Manufacturing and Advances in Wire Arc Additive Manufacturing of Aluminium, *Mater. Sci. Tech-lond.*, 2018, **34**(8), p 895–916
8. J.R. Kennedy, A.E. Davis, A.E. Caballero, S. Williams, E.J. Pickering and P.B. Prangnell, The Potential for Grain Refinement of Wire-Arc Additive Manufactured (WAAM) Ti-6Al-4V by ZrN and TiN Inoculation, *Addit. Manuf.*, 2021, **40**, p 101928
9. V.T. Le, D.S. Mai, T.K. Doan and H. Paris, Wire and Arc Additive Manufacturing of 308L Stainless Steel Components: Optimization of Processing Parameters and Material Properties, *Eng. Sci. Technol.*, 2021, **24**(4), p 1015–1026
10. X. Zuo, W. Zhang, Y. Chen, J.P. Oliveira, Z. Zeng, Y. Li, Z. Luo and S. Ao, Wire-Based Directed Energy Deposition of NiTiTa Shape Memory Alloys: Microstructure, Phase Transformation, Electrochemistry, X-Ray Visibility and Mechanical Properties, *Addit. Manuf.*, 2022, **59**, p 103115
11. S. Li, J.Y. Li, Z.W. Jiang, Y. Cheng, Y.Z. Li, S. Tang, J.Z. Leng, H.X. Chen, Y. Zou, Y.H. Zhao, J.P. Oliveira, Y. Zhang and K.H. Wang, Controlling the Columnar-To-Equiaxed Transition during Directed Energy Deposition of Inconel 625, *Addit. Manuf.*, 2022, **57**, p 102958
12. T.A. Rodrigues, V.R. Duarte, R.M. Miranda, T.G. Santos and J.P. Oliveira, Ultracold-Wire and Arc Additive Manufacturing (UC-WAAM), *J. Mater. Process Tech.*, 2021, **296**, p 117196
13. T.A. Rodrigues, F.W. Cipriano Farias, K. Zhang, A. Shamsolhodaei, J. Shen, N. Zhou, N. Schell, J. Capek, E. Polatidis, T.G. Santos and J.P. Oliveira, Wire and Arc Additive Manufacturing of 316L Stainless Steel/Inconel 625 Functionally Graded Material: Development and Characterization, *J. Mater. Res. Technol.*, 2022, **21**, p 237–251
14. Y. Song, W. Du, L. Zhao, L. Zeng, W. Liu, Y. Chen, B. Zhu, X. Zhang and X. Ding, The Coupling Influences and Corresponding Mechanisms of High Efficiency Thermal-Magnetic Treatments on the Dimensional Stability of Al-Cu-Mg Alloy, *J. Alloy Compd.*, 2022, **928**, p 167187
15. S. Mondol, U. Bansal, P. Dhanalakshmi, S.K. Makineni, A. Mandal and K. Chattopadhyay, Enhancement of High Temperature Strength of Al-Cu Alloys By Minor Alloying and Hot Working Process, *J. Alloy Compd.*, 2022, **921**, p 166136
16. J. Qin, P. Tan, X. Quan, Z. Liu, D. Yi and B. Wang, The Effect of sc Addition on Microstructure and Mechanical Properties of As-Cast Zr-Containing Al-Cu Alloys, *J. Alloy Compd.*, 2022, **909**, p 164686
17. Robotic welding solution achieves 64% reduction in cycle time, https://scottautomation.com/en-us/insights/drake-trailers
18. L.J. da Silva, F.M. Scotti, D.B. Fernandes, R.P. Reis and A. Scotti, Effect of O_2 Content in Argon-Based Shielding Gas on Arc Wandering in WAAM of Aluminum Thin Walls, *CIRP J. Manuf. Sci. Tec.*, 2021, **32**, p 338–345
19. C. Zhang, M. Gao and X. Zeng, Workpiece Vibration Augmented Wire Arc Additive Manufacturing of High Strength Aluminum Alloy, *J. Mater. Process Tech.*, 2019, **271**, p 85–92
20. J.Y. Bai, C.L. Yang, S.B. Lin, B.L. Dong and C.L. Fan, Mechanical Properties of 2219-Al Components Produced by Additive Manufacturing with TIG, *Inv. J. Adv. Manuf. Tech.*, 2015, **86**(1–4), p 479–485
21. K.F. Ayarkwa, S.W. Williams and J. Ding, Assessing the Effect of TIG Alternating Current Time Cycle on Aluminium Wire + Arc Additive Manufacture, *Addit. Manuf.*, 2017, **18**, p 186–193
22. F. Wang, S. Williams and M. Rush, Morphology Investigation on Direct Current Pulsed Gas Tungsten Arc Welded Additive Layer Manufactured Ti6Al4V Alloy, *Inv. J. Adv. Manuf. Tech.*, 2011, **57**(5–8), p 597–603
23. T. Artaza, A. Suárez, F. Veiga, I. Braceras, I. Tabernero, O. Larrañaga and A. Lamikiz, Wire Arc Additive Manufacturing Ti6Al4V Aeronautical Parts Using Plasma Arc Welding: Analysis of Heat-Treatment Processes in Different Atmospheres, *J. Mater. Res. Technol.*, 2020, **9**(6), p 15454–15466
24. J. Lin, Y. Lv, D. Guo, X. Wu, Z. Li, C. Liu, B. Guo, G. Xu and B. Xu, Enhanced Strength and Ductility in Thin Ti-6Al-4V Alloy Components by Alternating the Thermal Cycle Strategy during Plasma Arc Additive Manufacturing, *Mat. Sci. Eng. A-Struct.*, 2019, **759**, p 288–297
25. B.P. Nagasai, S. Malarvizhi and V. Balasubramanian, Effect of Welding Processes on Mechanical and Metallurgical Characteristics of Carbon Steel Cylindrical Components Made by Wire Arc Additive Manufacturing (WAAM) Technique, *CIRP J. Manuf. Sci. Tec.*, 2022, **36**, p 100–116
26. R. Warsi, K.H. Kazmi and M. Chandra, Mechanical Properties of Wire and Arc Additive Manufactured Component Deposited by a CNC Controlled GMAW, *Mater. Today Proc.*, 2022, **56**, p 2818–2825
27. S.S. Vaishnavan, K. Jayakuamr, P.N. Kumar and T. Suresh, Effect of ER5183 Filler Rod on the Metallurgical and Mechanical Roperties of TIG-Welded AA5083 and AA5754 Joints, *Mater. Today Proc.*, 2023, **72**(4), p 2251–2254
28. N. Rakesh, A. Mohan, P. Navaf, M.S. Harisankar, S.J. Nambiar, M. Harikrishnan, J.S. Devadathan and K. Rameshkumar, Effect of Fluxes on Weld Penetration during TIG Welding—A Review, *Mater. Today Proc.*, 2023, **72**(6), p 3040–3048
29. J.H. Ouyang, H. Wang and R. Kovacevic, Rapid Prototyping of 5356-Aluminum Alloy Based on Variable Polarity Gas Tungsten Arc

Welding: Process Control and Microstructure, *Mater. Manuf. Process.*, 2017, **17**(1), p 103–124
30. B. Dong, X. Cai, S. Lin, X. Li, C. Fan, C. Yang and H. Sun, Wire Arc Additive Manufacturing of Al-Zn-Mg-Cu Alloy: Microstructures and Mechanical Properties, *Addit. Manuf.*, 2020, **36**, p 101447
31. X. Cai, B. Dong, X. Yin, S. Lin, C. Fan and C. Yang, Wire Arc Additive Manufacturing of Titanium Aluminide Alloys Using Two-Wire TOP-TIG Welding: Processing, Microstructures, and Mechanical Properties, *Addit. Manuf.*, 2020, **35**, p 101344
32. X. Zhang, K. Wang, Q. Zhou, J. Ding, S. Ganguly, G. Marzio, D. Yang, X. Xu, P. Dirisu and S.W. Williams, Microstructure and Mechanical Properties of TOP-TIG-Wire and Arc Additive Manufactured Super Duplex Stainless Steel (ER2594), *Mat. Sci. Eng. A-Struct.*, 2019, **762**, p 138097
33. Z. Qi, B. Cong, B. Qi, H. Sun, G. Zhao and J. Ding, Microstructure and Mechanical Properties of Double-Wire + Arc Additively Manufactured Al-Cu-Mg Alloys, *J. Mater. Process Tech.*, 2018, **255**, p 347–353
34. Z. Yu, T. Yuan, M. Xu, H. Zhang, X. Jiang and S. Chen, Microstructure and Mechanical Properties of Al-Zn-Mg-Cu Alloy Fabricated by Wire + Arc Additive Manufacturing, *J. Manuf. Process.*, 2021, **62**, p 430–439
35. B. Cong, X. Cai, Z. Qi, B. Qi, Y. Zhang, R. Zhang, W. Guo, Z. Zhou, Y. Yin and X. Bu, The Effects of Ultrasonic Frequency Pulsed Arc on Wire + Arc Additively Manufactured High Strength Aluminum Alloys, *Addit. Manuf.*, 2022, **51**, p 102617
36. J. Lin, Y. Lv, Y. Liu, Z. Sun, K. Wang, Z. Li, Y. Wu and B. Xu, Microstructural Evolution and Mechanical Property of Ti-6Al-4V Wall Deposited by Continuous Plasma Arc Additive Manufacturing Without Post Heat Treatment, *J. Mech. Behav. Biomed.*, 2017, **69**, p 19–29
37. F.J. Xu, Y.H. Lv, B.S. Xu, Y.X. Liu, F.Y. Shu and P. He, Effect of Deposition Strategy on the Microstructure and Mechanical Properties of Inconel 625 Superalloy Fabricated by Pulsed Plasma Arc Deposition, *Mater. Des.*, 2013, **45**, p 446–455
38. K. Wang, Y. Liu, Z. Sun, J. Lin, Y. Lv and B. Xu, Microstructural Evolution and Mechanical Properties of Inconel 718 Superalloy Thin Wall Fabricated by Pulsed Plasma Arc Additive Manufacturing, *J. Alloy Compd.*, 2020, **819**, p 152936
39. A. Ty, Y. Balcaen, M. Mokhtari and J. Alexis, Influence of Deposit and Process Parameters on Microstructure and Mechanical Properties of Ti6Al4V Obtained by DED-W (PAW), *J. Mater. Res. Technol.*, 2022, **18**, p 2853–2869
40. C. Li, F. Jiang, B. Xu, G. Zhang, S. Chen, Z. Yan, B. Wang, S. Lin and C. Fan, In-Situ Measurement of the Droplet Temperature, Velocity and Mass Under Plasma Arc, *Measurement*, 2022, **202**, p 111905
41. S. Singh, V. Kumar, S. Kumar and A. Kumar, Variant of MIG Welding of Similar and Dissimilar Metals—A Review, *Mater. Today Proc.*, 2022, **56**, p 3550–3555
42. P. Wang, S. Hu, J. Shen and Y. Liang, Characterization the Contribution and Limitation of the Characteristic Processing Parameters in Cold Metal Transfer Deposition of an Al Alloy, *J. Mater. Process Tech.*, 2017, **245**, p 122–133
43. C.G. Pickin, S.W. Williams and M. Lunt, Characterisation of the Cold Metal Transfer (CMT) Process and its Application for Low Dilution Cladding, *J. Mater. Process Tech.*, 2011, **211**(3), p 496–502
44. B. Cong, R. Ouyang, B. Qi and J. Ding, Influence of Cold Metal Transfer Process and Its Heat Input on Weld Bead Geometry and Porosity of Aluminum-Copper Alloy Welds, *Rare Metal. Mat. Eng.*, 2016, **45**(3), p 606–611
45. S. Zhou, H. Xie, J. Ni, G. Yang, L. Qin and X. Guo, Metal Transfer Behavior during CMT-Based Wire Arc Additive Manufacturing of Ti-6Al-4V Alloy, *J. Manuf. Process.*, 2022, **82**, p 159–173
46. B. Cong, Z. Qi, B. Qi, H. Sun, G. Zhao and J. Ding, A Comparative Study of Additively Manufactured Thin Wall and Block Structure with Al-6.3%Cu Alloy Using Cold Metal Transfer Process, *Appl. Sci.*, 2017, **7**(3), p 275–286
47. J. Gu, J. Bai, J. Ding, S. Williams, L. Wang and K. Liu, Design and Cracking Susceptibility of Additively Manufactured Al-Cu-Mg Alloys with Tandem Wires and Pulsed Arc, *J. Mater. Process Tech.*, 2018, **262**, p 210–220
48. S.Y. Fan, X.P. Guo, Y. Tang and X.M. Guo, Microstructure and Mechanical Properties of Al-Cu-Mg Fabricated by Double-Wire CMT Arc Additive Manufacturing, *Metals*, 2022, **12**, p 416–427
49. S.C. Altıparmak, V.A. Yardley, Z. Shi and J. Lin, Challenges in Additive Manufacturing of High-Strength Aluminium Alloys and Current Developments in Hybrid Additive Manufacturing, *Int. J. Light. Mater. Manuf.*, 2021, **4**(2), p 246–261
50. Z. Zhang, C. Sun, X. Xu and L. Liu, Surface Quality and Forming Characteristics of Thin-Wall Aluminium Alloy Parts Manufactured by Laser Assisted MIG Arc Additive Manufacturing, *Int. J. Light. Mater. Manuf.*, 2018, **1**(2), p 89–95
51. Z. Zhang, Z. Ma, S. He, G. Song and L. Liu, Effect of Laser Power on the Microstructure and Mechanical Properties of 2319-Al Fabricated by Wire-Based Additive Manufacturing, *J. Mater. Eng. Perform.*, 2021, **30**(9), p 6640–6649
52. G. Liu, J. Xiong and L. Tang, Microstructure and Mechanical Properties of 2219 Aluminum Alloy Fabricated by Double-Electrode Gas Metal Arc Additive Manufacturing, *Addit. Manuf.*, 2020, **35**, p 101375
53. J. Wei, C. He, M. Qie, Y. Li, Y. Zhao, G. Qin and L. Zuo, Microstructure Refinement and Mechanical Properties Enhancement of Wire-Arc Additive Manufactured 2219 Aluminum Alloy Assisted by Interlayer Friction Stir Processing, *Vacuum*, 2022, **203**, p 111264
54. J. Wei, C. He, Y. Zhao, M. Qie, G. Qin and L. Zuo, Evolution of Microstructure and Properties in 2219 Aluminum Alloy Produced by Wire Arc Additive Manufacturing Assisted by Interlayer Friction Stir Processing, *Mater. Sci. Eng. A-Struct.*, 2023, **868**, p 144794
55. Z. Wang, X. Lin, L. Wang, Y. Cao, Y. Zhou and W. Huang, Microstructure Evolution and Mechanical Properties of the Wire + Arc Additive Manufacturing Al-Cu Alloy, *Addit. Manuf.*, 2021, **47**, p 102298
56. J. Gu, M. Gao, S. Yang, J. Bai, Y. Zhai and J. Ding, Microstructure, Defects, and Mechanical Properties of Wire + Arc Additively Manufactured Al Cu4.3-Mg1.5 Alloy, *Mater. Des.*, 2020, **186**, p 108357
57. Y. Zhou, X. Lin, N. Kang, Z. Wang, H. Tan and W. Huang, Hot Deformation Induced Microstructural Evolution in Local-Heterogeneous Wire + Arc Additive Manufactured 2219 Al Alloy, *J. Alloy Compd.*, 2021, **865**, p 158949
58. J.Y. Bai, C.L. Fan, S.B. Lin, C.L. Yang and B.L. Dong, Effects of Thermal Cycles on Microstructure Evolution of 2219-Al during GTA-Additive Manufacturing, *Inv. J. Adv. Manuf. Tech.*, 2016, **87**(9–12), p 2615–2623
59. T.A. Rodrigues, J.D. Escobar, J. Shen, V.R. Duarte, G.G. Ribamar, J.A. Avila, E. Maawad, N. Schell, T.G. Santos and J.P. Oliveira, Effect of Heat Treatments on 316 Stainless Steel Parts Fabricated by Wire and Arc Additive Manufacturing: Microstructure and Synchrotron X-Ray Diffraction Analysis, *Addit. Manuf.*, 2021, **48**, p 102428
60. B. Bevans, A. Ramalho, Z. Smoqi, A. Gaikwad, T.G. Santos, P. Rao and J.P. Oliveira, Monitoring and Flaw Detection During Wire-Based Directed Energy Deposition Using In-Situ Acoustic Sensing and Wavelet Graph Signal Analysis, *Mater. Des.*, 2023, **225**, p 111480
61. J. Shi, F. Li, S. Chen, Y. Zhao and H. Tian, Effect of in-Process Active Cooling on Forming Quality and Efficiency of Tandem GMAW–Based Additive Manufacturing, *Inv. J. Adv. Manuf. Tech.*, 2018, **101**(5–8), p 1349–1356
62. M. Köhler, J. Hensel and K. Dilger, Effects of Thermal Cycling on Wire and Arc Additive Manufacturing of Al-5356 Components, *Metals*, 2020, **10**(7), p 952–963
63. Z. Wang, X. Lin, N. Kang, J. Chen, H. Tan, Z. Feng, Z. Qin, H. Yang and W. Huang, Laser Powder Bed Fusion of High-Strength Sc/Zr-Modified Al-Mg Alloy: Phase Selection, Microstructural/Mechanical Heterogeneity, and Tensile Deformation Behavior, *J. Mater. Sci. Technol.*, 2021, **95**, p 40–56
64. M. Gaumann, C. Bezencon, P. Canalis and W. Kurz, Single-Crystal Laser Deposition of Superalloys: Processing-Microstructure Maps, *Acta Mater.*, 2001, **49**, p 1051–1062
65. Y. Hu, S. Wu, Y. Guo, Z. Shen, A.M. Korsunsky, Y. Yu, X. Zhang, Y. Fu, Z. Che, T. Xiao, S. Lozano-Perez, Q. Yuan, X. Zhong, X. Zeng, G. Kang and P.J. Withers, Inhibiting Weld Cracking in High-Strength Aluminium Alloys, *Nat. Commun.*, 2022, **13**(1), p 5816
66. Y. Ma, Y. Huang and X. Zhang, Precipitation Thermodynamics and Kinetics of the Second Phase of Al-Zn-Mg-Cu-Sc-Zr-Ti Aluminum Alloy, *J. Mater. Res. Technol.*, 2021, **10**, p 445–452

67. J. Gu, J. Ding, S.W. Williams, H. Gu, J. Bai, Y. Zhai and P. Ma, The Strengthening Effect of Inter-Layer Cold Working and Post-Deposition Heat Treatment on the Additively Manufactured Al–6.3Cu Alloy, *Mat. Sci. Eng. A-Struct.*, 2016, **651**, p 18–26
68. Y. Zhou, X. Lin, N. Kang, W. Huang, J. Wang and Z. Wang, Influence of Travel Speed on Microstructure and Mechanical Properties of Wire + Arc Additively Manufactured 2219 Aluminum Alloy, *J. Mater. Sci. Technol.*, 2020, **37**, p 143–153
69. Y. Zhou, X. Lin, N. Kang, W. Huang and Z. Wang, Mechanical Properties and Precipitation Behavior of the Heat-Treated Wire + Arc Additively Manufactured 2219 Aluminum Alloy, *Mater. Charact.*, 2021, **171**, p 110735
70. M. Xu, S. Chen, T. Yuan, X. Jiang and H. Zhang, Effect of Thermal Cycles on the Microstructure and Properties of the Al-Zn-Mg-Cu Alloy during Wire-Arc Additive Manufacturing, *J. Alloy Compd.*, 2022, **928**, p 167172
71. H. Wang, Y. Yi and S. Huang, Influence of Pre-Deformation and Subsequent Ageing on the Hardening Behavior and Microstructure of 2219 Aluminum Alloy Forgings, *J. Alloy Compd.*, 2016, **685**, p 941–948
72. C. Su, X. Chen, C. Gao and Y. Wang, Effect of Heat Input on Microstructure and Mechanical Properties of Al-Mg Alloys Fabricated by WAAM, *Appl. Surf. Sci.*, 2019, **486**, p 431–440
73. A.H. Eftekhar, S.M. Sadrossadat and M. Reihanian, Effect of Heat Input on Microstructure and Mechanical Properties of TIG-Welded Semisolid Cast AXE622 Mg Alloy, *Mater. Charact.*, 2022, **184**, p 111692
74. P. Wang, H. Zhang, H. Zhu, Q. Li and M. Feng, Wire-Arc Additive Manufacturing of AZ31 Magnesium Alloy Fabricated by Cold Metal Transfer Heat Source: Processing, Microstructure, and Mechanical Behavior, *J. Mater. Process Tech.*, 2021, **288**, p 116895
75. J. Xiong, Y. Li, R. Li and Z. Yin, Influences of Process Parameters on Surface Roughness of Multi-Layer Single-Pass Thin-Walled Parts in GMAW-Based Additive Manufacturing, *J. Mater. Process Tech.*, 2018, **252**, p 128–136
76. A. Ramalho, T.G. Santos, B. Bevans, Z. Smoqi, P. Rao and J.P. Oliveira, Effect of Contaminations on the Acoustic Emissions during Wire and Arc Additive Manufacturing of 316L Stainless Steel, *Addit. Manuf.*, 2022, **51**, p 102585
77. F.W.C. Farias, V.R. Duarte, I.O. Felice, J.D.C.P. Filho, N. Schell, E. Maawad, J.A. Avila, J.Y. Li, Y. Zhang, T.G. Santos and J.P. Oliveira, In Situ Interlayer Hot Forging Arc-Based Directed Energy Deposition of Inconel® 625: Process Development and Microstructure Effects, *Addit. Manuf.*, 2023, **66**, p 103476
78. F.M. Ghaini, M. Sheikhi, M.J. Torkamany and J. Sabbaghzadeh, The Relation Between Liquation and Solidification Cracks in Pulsed Laser Welding of 2024 Aluminium Alloy, *Mater. Sci. Eng. A-Struct.*, 2009, **519**(1–2), p 167–171
79. J. Liu and S. Kou, Susceptibility of Ternary Aluminum Alloys to Cracking during Solidification, *Acta Mater.*, 2017, **125**, p 513–523
80. M. Opprecht, J.P. Garandet, G. Roux, C. Flament and M. Soulier, A Solution to the Hot Cracking Problem for Aluminium Alloys Manufactured by Laser Beam Melting, *Acta Mater.*, 2020, **197**, p 40–53
81. S.M. Dar, H. Liao and A. Xu, Effect of Cu and Mn Content on Solidification Microstructure, T-Phase Formation and Mechanical Property of Al Cu Mn Alloys, *J. Alloy Compd.*, 2019, **774**, p 758–767
82. T.V. Atamanenko, D.G. Eskin, M. Sluiter and L. Katgerman, On the Mechanism of Grain Refinement in Al-Zr-Ti Alloys, *J. Alloy Compd.*, 2011, **509**, p 57–60
83. Q. Zheng, C. Yang, S. Wang, A. Yu, H. Chen and Y. He, Effect of Compound Inoculants Ti and Zr on as Cast Microstructure and Mechanical Properties of Al-Cu Alloy, *Mater. Res. Innov.*, 2014, **18**(2), p 2–59
84. S. Zhou, K. Wu, G. Yang, B. Wu, L. Qin, H. Wu and C. Yang, Microstructure and Mechanical Properties of Wire Arc Additively Manufactured 205A High Strength Aluminum Alloy: The Comparison of As-Deposited and T6 Heat-Treated Samples, *Mater. Charact.*, 2022, **189**, p 111990
85. M.Y. Dong, Y. Zhao, Q. Li, F.D. Wang and A.P. Wu, Effects of Cd Addition in Welding Wires on Microstructure and Mechanical Property of Wire and Arc Additively Manufactured Al-Cu Alloy, *Trans. Nonferrous Met. Soc. China*, 2022, **32**(3), p 750–764
86. S. Wang, H.M. Gu, W. Wang, C.D. Li, L.L. Ren, Z.B. Wang, Y.C. Zhai and P.H. Ma, Microstructure and Properties of an Al-Cu-Sn Wall Deposited by Wire + Arc Additive Manufacturing, *Rare Metal Mater. Eng.*, 2021, **50**(1), p 0095–0101
87. C. Brice, R. Shenoy, M. Kral and K. Buchannan, Precipitation Behavior of Aluminum Alloy 2139 Fabricated Using Additive Manufacturing, *Mat. Sci. Eng. A-Struct.*, 2015, **648**, p 9–14
88. A. Kumar Sinha, S. Pramanik and K.P. Yagati, Research Progress in Arc Based Additive Manufacturing of Aluminium Alloys—A Review, *Measurement*, 2022, **200**, p 111672
89. R. Geng, J. Du, Z. Wei and N. Ma, Multiscale Modelling of Microstructure, Micro-Segregation, and Local Mechanical Properties of Al-Cu Alloys in Wire and Arc Additive Manufacturing, *Addit. Manuf.*, 2020, **36**, p 101735
90. P. Jin, Y. Liu, F. Li and Q. Sun, Realization of Synergistic Enhancement for Fracture Strength and Ductility by Adding TiC Particles in Wire and Arc Additive Manufacturing 2219 Aluminium Alloy, *Compos. Part B-Eng.*, 2021, **219**, p 108921
91. T. Hauser, R.T. Reisch, P.P. Breese, B.S. Lutz, M. Pantano, Y. Nalam, K. Bela, T. Kamps, J. Volpp and A.F.H. Kaplan, Porosity in Wire Arc Additive Manufacturing of Aluminium Alloys, *Addit. Manuf.*, 2021, **41**, p 101993
92. E.M. Ryan, T.J. Sabin, J.F. Watts and M.J. Whiting, The Influence of Build Parameters and Wire Batch on Porosity of Wire and Arc Additive Manufactured Aluminium Alloy 2319, *J. Mater. Process Tech.*, 2018, **262**, p 577–584
93. K.S. Derekar, A. Addison, S.S. Joshi, X. Zhang, J. Lawrence, L. Xu, G. Melton and D. Griffiths, Effect of Pulsed Metal Inert Gas (pulsed-MIG) and Cold Metal Transfer (CMT) Techniques on Hydrogen Dissolution in Wire Arc Additive Manufacturing (WAAM) of Aluminium, *Inv. J. Adv. Manuf. Tech.*, 2020, **107**(1–2), p 311–331
94. J. Gu, M. Gao, S. Yang, J. Bai, J. Ding and X. Fang, Pore Formation and Evolution in Wire + Arc Additively Manufactured 2319 Al Alloy, *Addit. Manuf.*, 2019, **30**, p 100900
95. Z. Wang, Y. Gao, J. Huang, C. Wu, G. Wang and J. Liu, Precipitation Phenomena and Strengthening Mechanism of Al-Cu Alloys Deposited by In-Situ Rolled Wire-Arc Additive Manufacturing, *Mat. Sci. Eng. A-Struct.*, 2022, **855**, p 143770
96. J. Gu, J. Ding, S.W. Williams, H. Gu, P. Maamd and Y. Zhai, The Effect of Inter-Layer Cold Working and Post-Deposition Heat Treatment on Porosity in Additively Manufactured Aluminum Alloys, *J. Mater. Process Tech.*, 2016, **230**, p 26–34
97. J. Fixter, J. Gu, J. Ding, S.W. Williams and P.B. Prangnell, Preliminary Investigation into the Suitability of 2xxx Alloys for Wire-Arc Additive Manufacturing, *Mater. Sci. Forum*, 2016, **877**, p 611–616
98. Y. Chi, N. Murali, T. Zheng, J. Liu and X. Li, Wire-Arc Additive Manufacturing of Nano-Treated Aluminum Alloy 2024, 3D Print, *Addit. Manuf.*, 2022 https://doi.org/10.1089/3dp.2022.0150
99. M. Sokoluk, C. Cao, S. Pan and X. Li, Nanoparticle-Enabled Phase Control for Arc Welding of Unweldable Aluminum Alloy 7075, *Nat. Commun.*, 2019, **10**(1), p 98
100. Z. Qi, B. Qi, B. Cong, H. Sun, G. Zhaoamd and J. Ding, Microstructure and Mechanical Properties of Wire + Arc Additively Manufactured 2024 Aluminum Alloy Components: As-Deposited and Post Heat-Treated, *J. Manuf. Process.*, 2019, **40**, p 27–36
101. Z. Barsoum and I. Barsoum, Residual Stress Effects on Fatigue Life of Welded Structures Using LEFM, *Eng. Fail. Anal.*, 2009, **16**(1), p 449–467
102. J. Ding, P. Colegrove, J. Mehnen, S. Ganguly, P.M. Sequeira Almeida, F. Wang and S. Williams, Thermo-Mechanical Analysis of Wire and Arc Additive Layer Manufacturing Process on Large Multi-Layer Parts, *Comput. Mater. Sci.*, 2011, **50**(12), p 3315–3322
103. M.M. Tawfik, M.M. Nemat-Alla and M.M. Dewidar, Enhancing the Properties of Aluminum Alloys Fabricated Using Wire + Arc Additive Manufacturing Technique—A Review, *J. Mater. Res. Technol.*, 2021, **13**, p 754–768
104. W.J. Sames, F.A. List, S. Pannala, R.R. Dehoff and S.S. Babu, The Metallurgy and Processing Science of Metal Additive Manufacturing, *Int. Mater. Rev.*, 2016, **61**(5), p 315–360
105. S. Wang, H. Gu, W. Wang, C. Li, L. Ren, Z. Wang, Y. Zhai and P. Ma, The Influence of Heat Input on the Microstructure and Properties of Wire-Arc-Additive-Manufactured Al-Cu-Sn Alloy Deposits, *Metals*, 2020, **10**(1), p 79–91

106. T. DebRoy, H.L. Wei, J.S. Zuback, T. Mukherjee, J.W. Elmer, J.O. Milewski, A.M. Beese, A. Wilson-Heid, A. De and W. Zhang, Additive Manufacturing of Metallic Components-Process, Structure and Properties, *Prog. Mater. Sci.*, 2018, **92**, p 112–224
107. R. Sun, L. Li, Y. Zhu, W. Guo, P. Peng, B. Cong, J. Sun, Z. Che, B. Li, C. Guo and L. Liu, Microstructure, Residual Stress and Tensile Properties Control of Wire-Arc Additive Manufactured 2319 Aluminum Alloy with Laser Shock Peening, *J. Alloy Compd.*, 2018, **747**, p 255–265
108. C. Wang, Y. Li, W. Tian, J. Hu, B. Li, P. Li and W. Liao, Influence of Ultrasonic Impact Treatment and Working Current on Microstructure and Mechanical Properties of 2219 Aluminium Alloy Wire Arc Additive Manufacturing Parts, *J. Mater. Res. Technol.*, 2022, **21**, p 781–797
109. J.R. Hönnige, P.A. Colegrove, S. Ganguly, E. Eimer, S. Kabra and S. Williams, Control of Residual Stress and Distortion in Aluminium Wire + Arc Additive Manufacture with Rolling, *Addit. Manuf.*, 2018, **22**, p 775–783
110. K.S. Derelar, B.L. Ahmad, X. Zhang, S.S. Joshi, J. Lawrence, L. Xu, G. Melton and A. Addison, Effects of Process Variants on Residual Stresses in Wire Arc Additive Manufacturing of Aluminum Alloy 5183, *J. Manuf. Sci E-T ASME*, 2022, **144**, p 071005
111. X. Fang, L. Zhang, G. Chen, K. Huang, F. Xue, L. Wang, J. Zhao and B. Lu, Microstructure Evolution of Wire-Arc Additively Manufactured 2319 Aluminum Alloy with Interlayer Hammering, *Mat. Sci. Eng. A-Struct.*, 2021, **800**, p 140168
112. Y.D. Wang, H.B. Tang, Y.L. Fang and H.M. Wang, Effect of Heat Treatment on Microstructure and Mechanical Properties of Laser Melting Deposited 1Cr12Ni2WMoVNb Steel, *Mater. Sci. Eng. A-Struct.*, 2010, **528**(1), p 474–479
113. Z. Qi, B. Cong, B. Qi, G. Zhao and J. Ding, Properties of Wire + Arc Additively Manufactured 2024 Aluminum Alloy with Different Solution Treatment Temperature, *Mater. Lett.*, 2018, **230**, p 275–278
114. J. Gu, S. Yang, M. Gao, J. Bai, Y. Zhai and J. Ding, Micropore Evolution In Additively Manufactured Aluminum Alloys Under Heat Treatment And Inter-Layer Rolling, *Mater. Des.*, 2020, **186**, p 108288
115. J. Gu, X. Wang, J. Bai, J. Ding, S. Williams, Y. Zhai and K. Liu, Deformation Microstructures and Strengthening Mechanisms for the Wire+Arc Additively Manufactured Al-Mg45Mn Alloy with Inter-Layer Rolling, *Mater. Sci. Eng. A-Struct.*, 2018, **712**, p 292–301
116. J. Zhou, X. Zhou, H. Li, J. Hu, X. Han and S. Liu, In-Situ Laser Shock Peening for Improved Surface Quality and Mechanical Properties of Laser-Directed Energy-Deposited AlSi10Mg Alloy, *Addit. Manuf.*, 2022, **60**, p 103177
117. A. Feng, Y. Wei, B. Liu, C. Chen, X. Pan and J. Xue, Microstructure and Mechanical Properties of Composite Strengthened High-Chromium Cast Iron by Laser Quenching and Laser Shock Peening, *J. Mater. Res. Technol.*, 2022, **20**, p 4342–4355
118. M. Diao, C. Guo, Q. Sun, F. Jiang, L. Li, J. Li, D. Xu, C. Liu and H. Song, Improving Mechanical Properties of Austenitic Stainless Steel by the Grain Refinement in Wire and Arc Additive Manufacturing Assisted with Ultrasonic Impact Treatment, *Mat. Sci. Eng. A-Struct.*, 2022, **857**, p 144044
119. Q. Tan, J. Zhang, Q. Sun, Z. Fan, G. Li, Y. Yin, Y. Liu and M.X. Zhang, Inoculation Treatment of an Additively Manufactured 2024 Aluminium Alloy with Titanium Nanoparticles, *Acta Mater.*, 2020, **196**, p 1–16
120. X. Liu, Y. Liu, Z. Zhou, K. Wang, Q. Zhan and X. Xiao, Grain Refinement and Crack Inhibition of Selective Laser Melted AA2024 Aluminum Alloy Via Inoculation with TiC-TiH2, *Mater. Sci. Eng. A-Struct.*, 2021, **813**, p 141171
121. J.Y. Bai, C.L. Fan, S.B. Lin, C.L. Yang and B.L. Dong, Mechanical Properties and Fracture Behaviors of GTA-Additive Manufactured 2219-Al After an Especial Heat Treatment, *J. Mater. Eng. Perform.*, 2017, **26**(4), p 1808–1816